Quantum optics and information with trapped ions

- Introduction to ion trapping and cooling
- Trapped ions as qubits for quantum computing and simulation
- Rydberg excitations for fast entangling operations
- Quantum thermodynamics, Kibble Zureck law, and heat engines
- Implanting single ions for a solid state quantum device

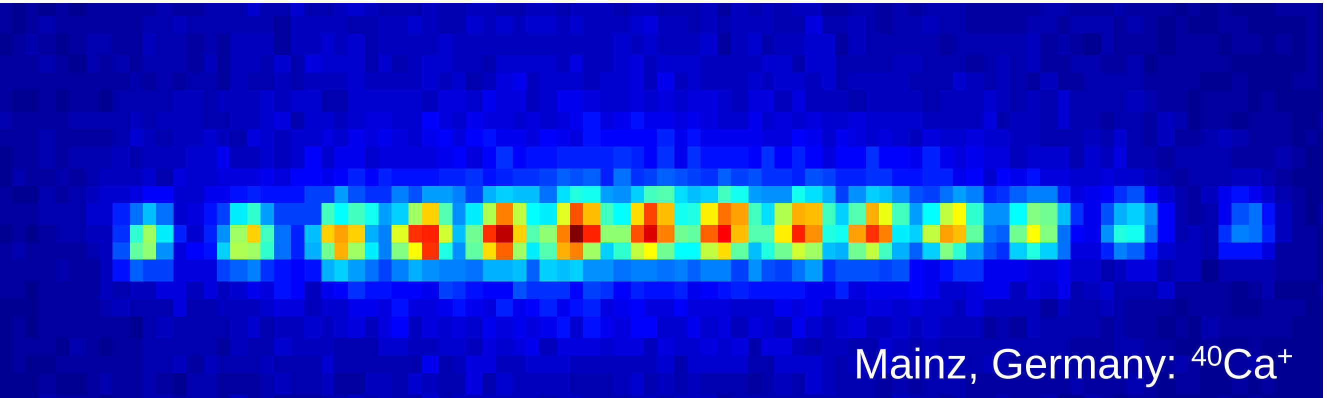

www.quantenbit.de
F. Schmidt-Kaler
JG|U
JOHANNES GUTENBERG UNIVERSITÄT MAINZ

Ion Gallery

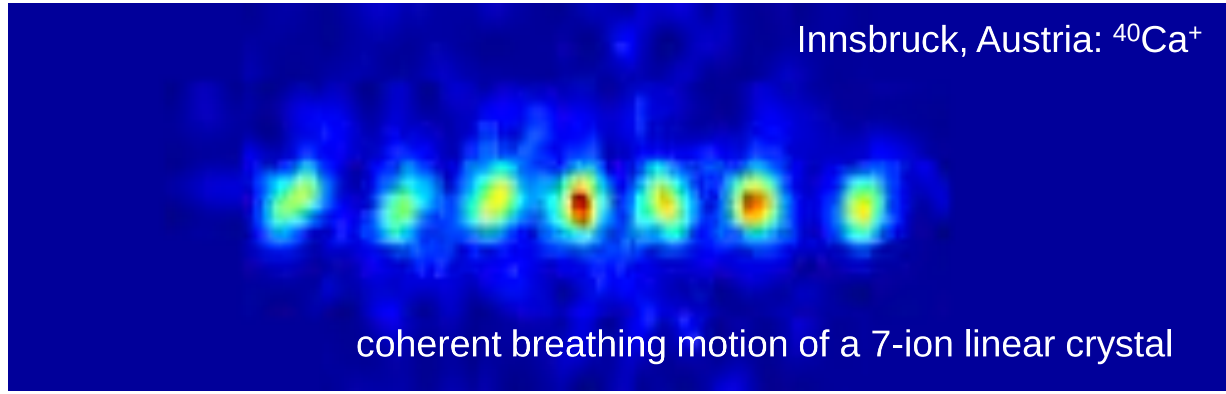

Innsbruck, Austria: $^{40}Ca^{+}$

coherent breathing motion of a 7-ion linear crystal

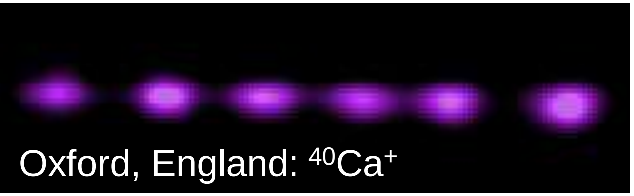

Oxford, England: $^{40}Ca^{+}$

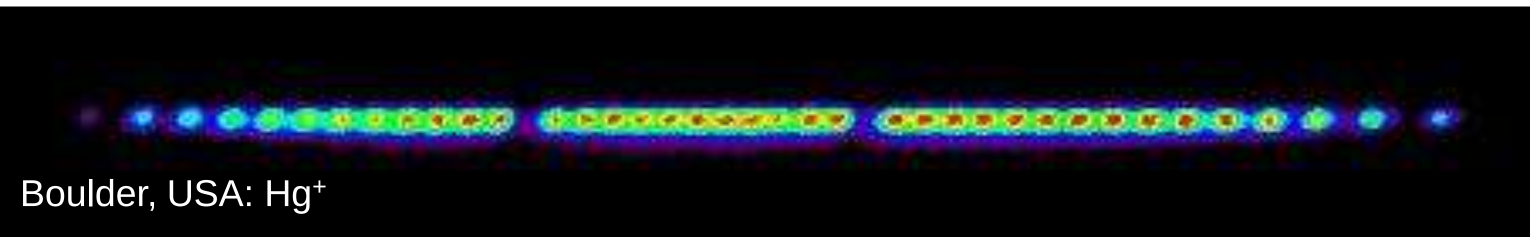

Boulder, USA: Hg^{+}

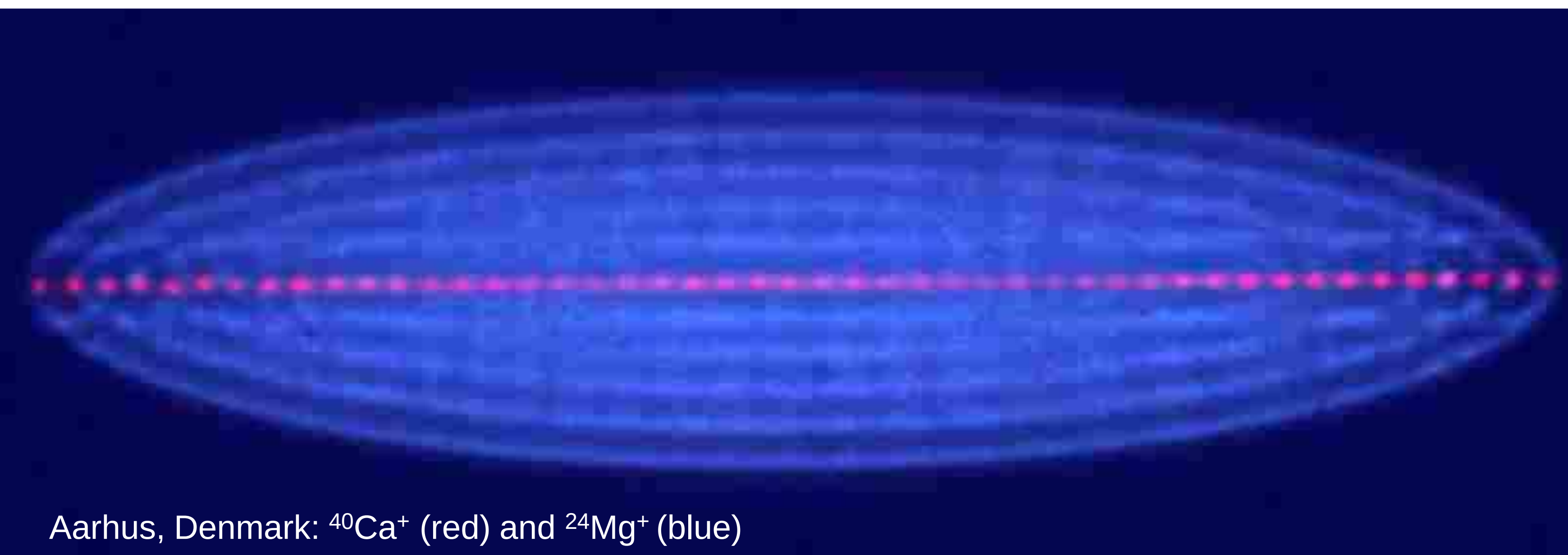

Aarhus, Denmark: $^{40}Ca^{+}$ (red) and $^{24}Mg^{+}$ (blue)

Why using ions?

- Ions in Paul traps were the first sample with which laser cooling was demonstrated and quite some Nobel prizes involve laser cooling…

- A single laser cooled ion still represents one of the best understood objects for fundamental investigations of the interaction between matter and radiation

- Experiments with single ions spurred the development of similar methods with neutral atoms

- Particular advantages of ions are that they are
  - confined to a very small spatial region ($\delta x<\lambda$)
  - controlled and measured at will for experimental times of days

- Ideal test ground for fundamental quantum optical experiments

- Further applications for
  - precision measurements
  - cavity QED
  - optical clocks
  - quantum computing
  - thermodynamics with small systems
  - quantum phase transitions

Introduction to ion trapping

Paul trap in 3D
Linear Paul trap

micro traps:
segmented linear trap
planar segmented trap

Eigenmodes of a linear ion crystal
Stability of a linear crystal

planar ion crystals
non-harmonic contributions

Micromotion

Modern segmented micro Paul trap

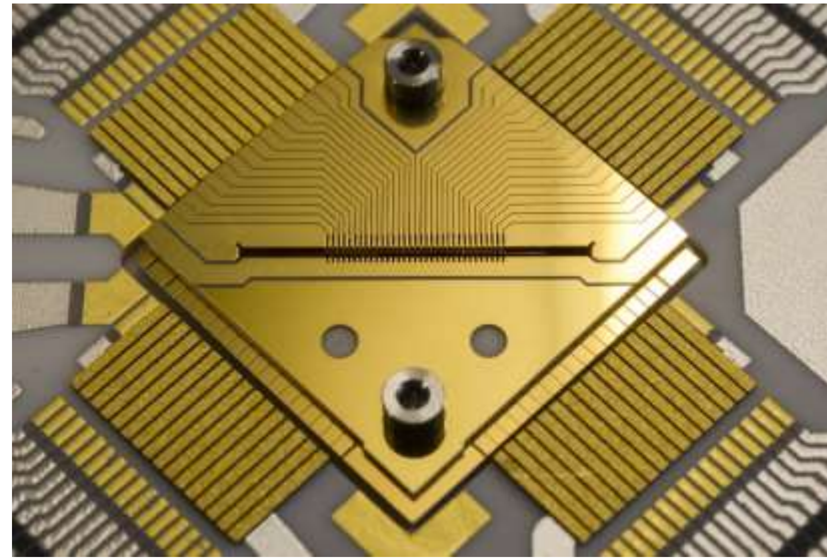

Traditional Paul trap

Dynamic confinement in Paul trap

Invention of the Paul trap

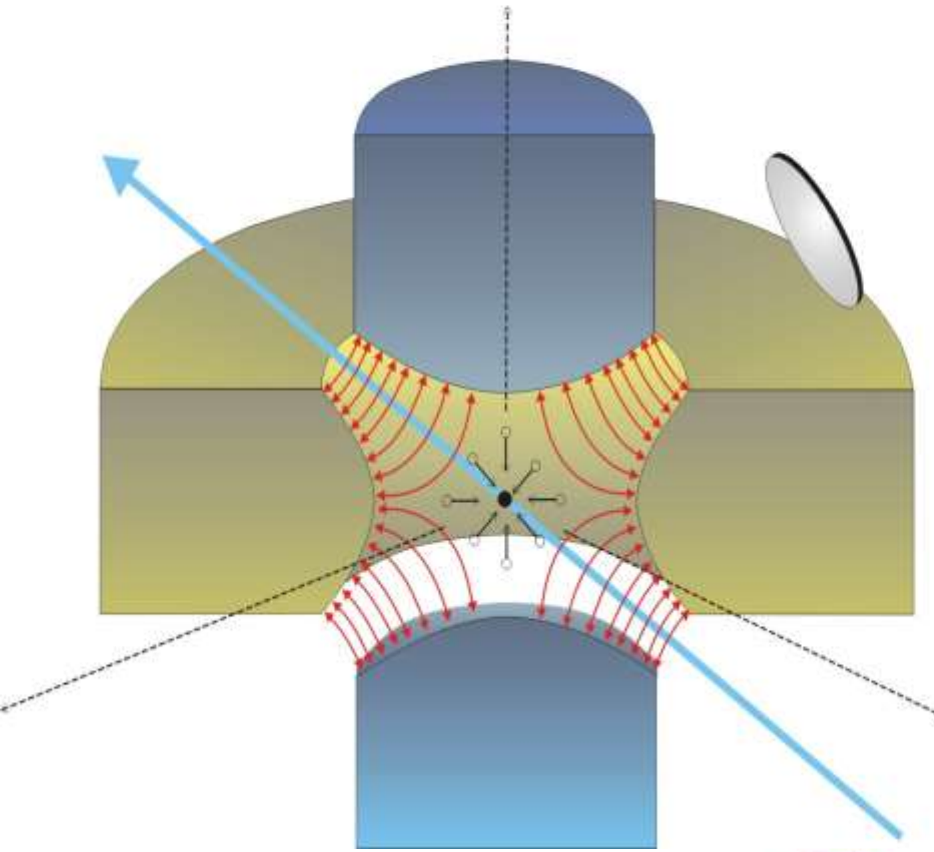

Wolfgang Paul (Nobel prize 1989)

DK 537.534.3 535.336.2

FORSCHUNGSBERICHTE
DES WIRTSCHAFTS- UND VERKEHRSMINISTERIUMS
NORDRHEIN-WESTFALEN

Herausgegeben von Staatssekretär Prof. Dr. h. c. Dr. E. h. Leo Brandt

Nr. 415

Prof. Dr.-Ing. Wolfgang Paul
Dr. rer. nat. Otto Osberghaus
Dipl.-Phys. Erhardt Fischer
Physikalisches Institut der Universität Bonn

Ein Ionenkäfig

Als Manuskript gedruckt

WESTDEUTSCHER VERLAG / KÖLN UND OPLADEN
1958

Binding in three dimensions

Electrical quadrupole potential $\Phi(\vec{r}) = \Phi_0 \cdot \sum \alpha_i (r_i/\tilde{r})^2, \quad i = x, y, z$

trap size: $\tilde{r}$

Binding force for charge Q $\vec{F}(\vec{r}) = Q\vec{E}(\vec{r}) = -Q\vec{\nabla}\Phi$

leads to a harmonic binding: $\vec{F}(\vec{r}) \sim \vec{r}$

Ion confinement requires a focusing force in 3 dimensions, but

Laplace equation requires $\vec{\nabla}^2\Phi = (\partial^2/\partial x^2 + \partial^2/\partial y^2 + \partial^2/\partial z^2)\Phi = 0$

such that at least one of the coefficients α_i is negative,
e.g. binding in x- and y-direction but anti-binding in z-direction !

no static trapping in 3 dimensions

Dynamical trapping: Paul's idea

time depending potential $\Phi(\overrightarrow{r}, t) = \Phi_0(t) \cdot (x^2 + y^2 - 2z^2)$

with $\Phi_0(t) = (U + V cos(\Omega_{RF} t))/\tilde{r}^2$

leads to the equation of motion for a particle with charge *Q* and mass *m*

$$\ddot{r}_i + \frac{2\alpha_i Q}{m r_0^2} \; \frac{U + V cos(\Omega_{RF} t)}{\tilde{r}^2} \; r_i = 0, \;\; \alpha_{x,y} = 1, \alpha_z = 2,$$

takes the standard form of the *Mathieu* equation
(linear differential equ. with time depending cofficients)

$$\boxed{\frac{d^2 u}{d\tau^2} + (a + 2\,q\,cos(2\tau))u = 0}$$

with substitutions

$$a_z = -2a_r = -\frac{8QU}{m\tilde{r}^2\Omega_{RF}^2} \qquad q_z = -2q_r = -\frac{4QV}{m\tilde{r}^2\Omega_{RF}^2}$$

radial and axial trap radius $\tilde{r}^2 = r_0^2 + 2z_0^2$ $\qquad \tau = \frac{1}{2}\Omega_{RF} t$

Mechanical Paul trap

Rotating saddle

$$\Phi(x,y,t) = \Phi_0(t) \cdot (x^2 - y^2)$$

Stable confinement of a ball in the rotating potential

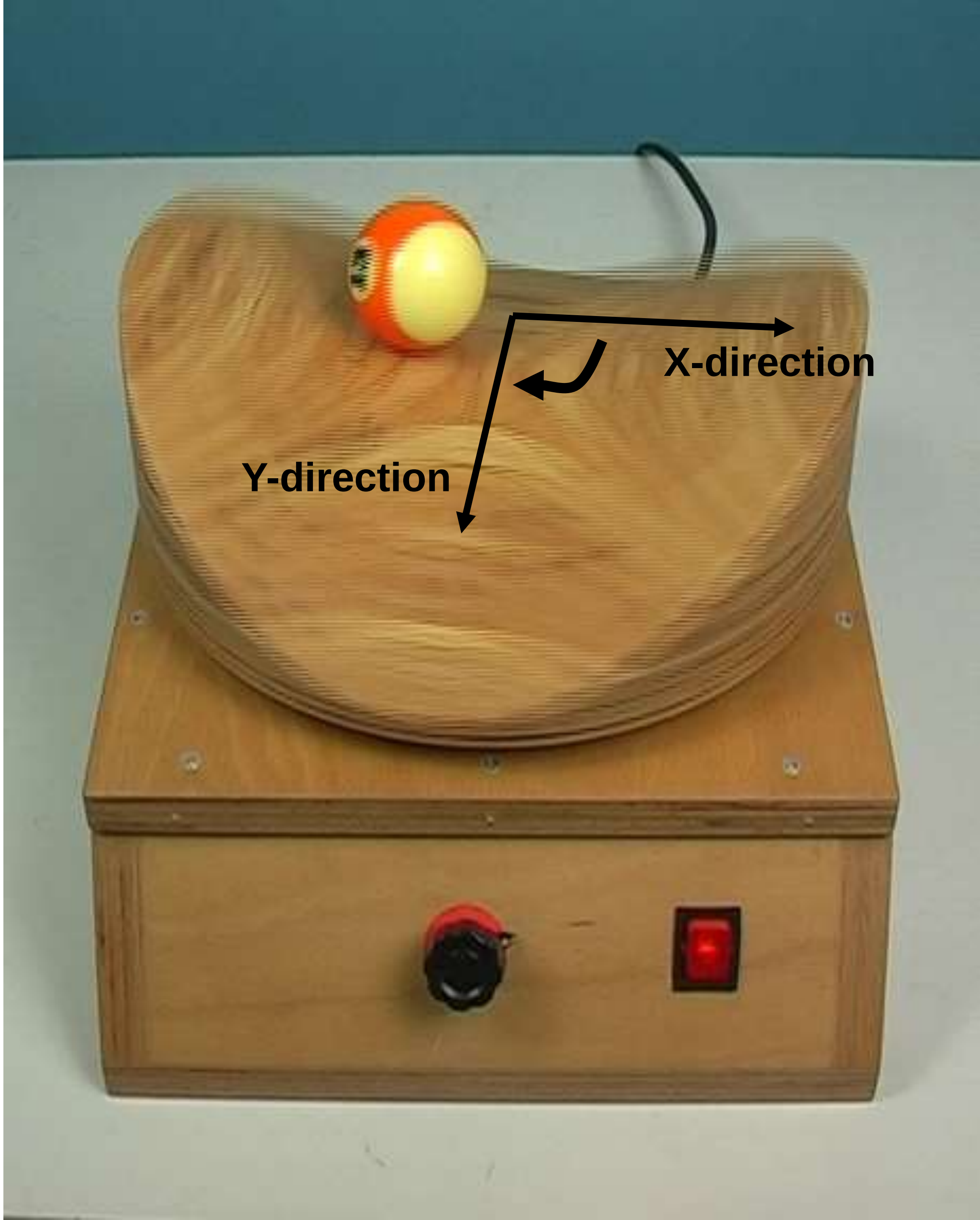

Regions of stability

time-periodic diff. equation leads to Floquet Ansatz

$$x(\tau) = Ae^{+i\mu\tau}\,\phi(\tau) + Be^{-i\mu\tau}\,\phi(\tau), \qquad \phi(\tau) = \phi(\tau+\pi) = \sum c_n e^{2in\tau}$$

If the exponent μ is purely real, the motion is bound,
if μ has some imaginary part x is exponantially growing and the motion is unstable.

The parameters *a* and *q* determine if the motion is stable or not.
Find solution analytically (complicated) or numerically:

a=0, *q* =0.9

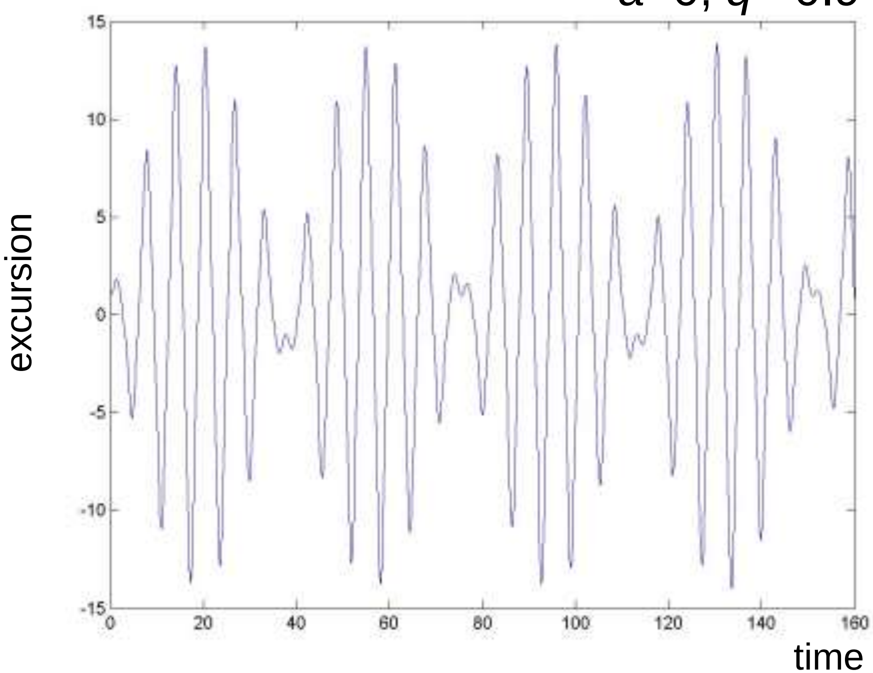

a=0, *q* =1.0

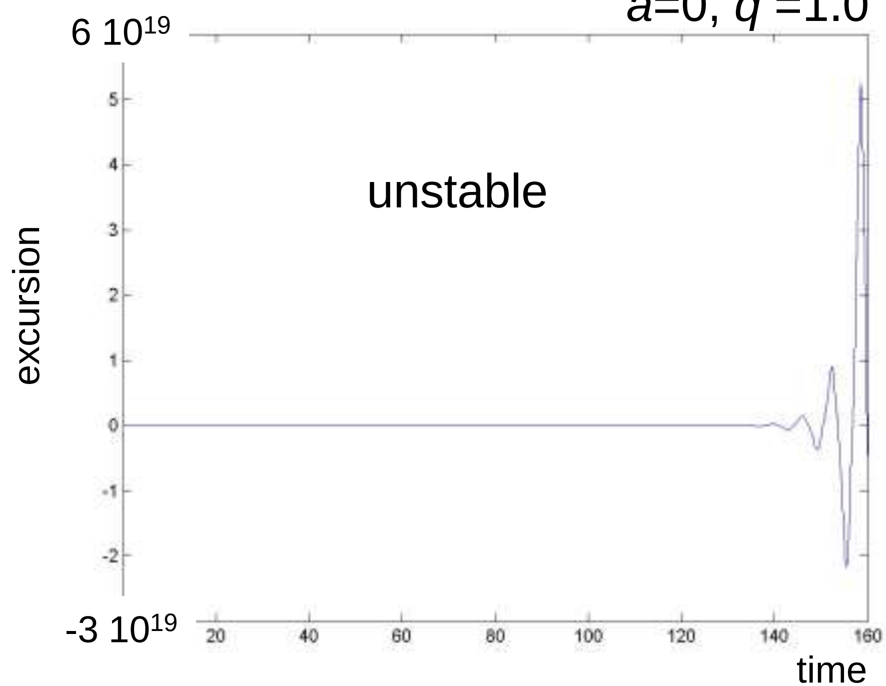

Two oscillation frequencies

slow frequency: Harmonic secular motion, frequency ω increases with increasing q

fast frequency: Micromotion with frequency Ω
Ion is shaken with the RF drive frequency (disappears at trap center)

1D-solution of Mathieu equation

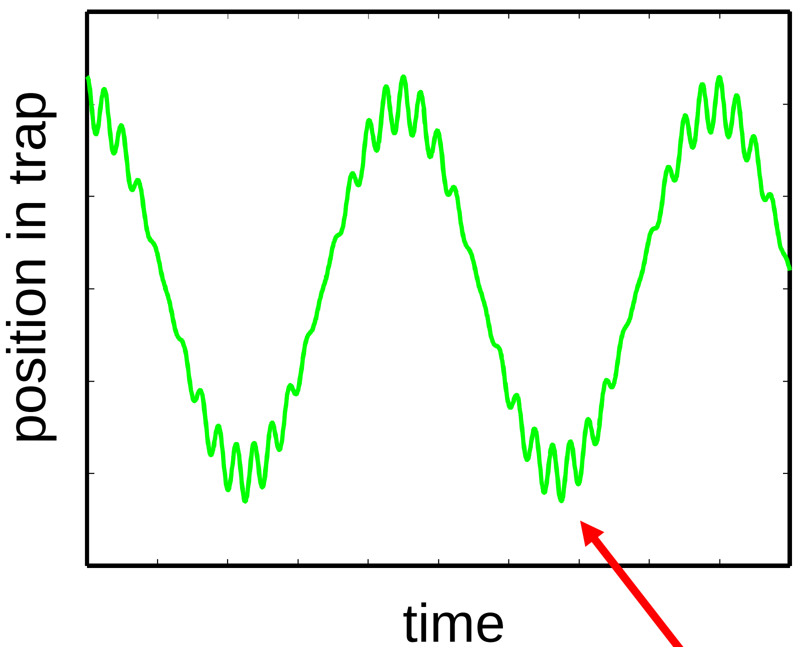

single Aluminium dust particle in trap

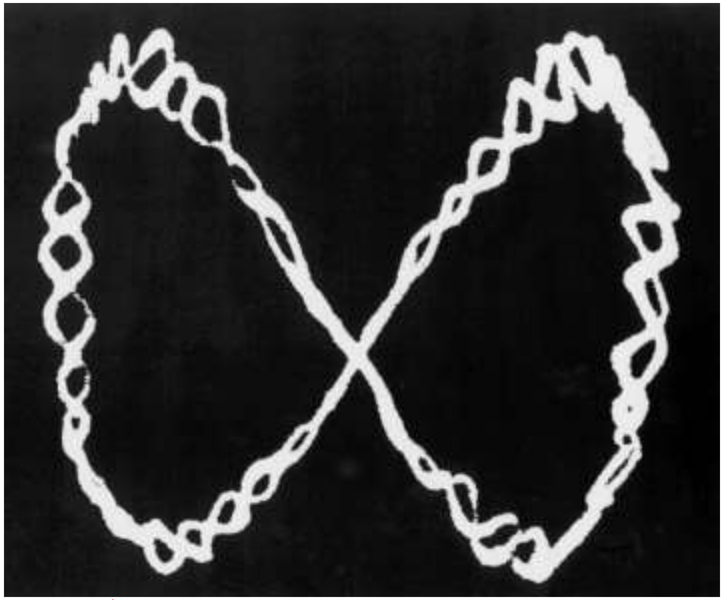

Lissajous figure

micromotion

3-Dim. Paul trap stability diagram

for a << q << 1 exist approximate solutions

$$r_i(t) = r_1^0 cos(\omega_1 t + \phi_i)(1 + \frac{q_i}{2} cos(\Omega_{RF} t))$$

$$\boxed{\begin{aligned} \omega_i &= \beta_i \frac{\Omega_{RF}}{2} \\ \beta_i &= \sqrt{a_i + \frac{q_i}{2}} \end{aligned}}$$

The 3D harmonic motion with frequency ω_i can be interpreted, approximated, as being caused by a pseudo-potential Ψ

$$\boxed{Q\Psi = \frac{1}{2} \sum m\omega_i^2 r_i^2, \quad i = x, y, z}$$

→ leads to a quantized harmonic oscillator

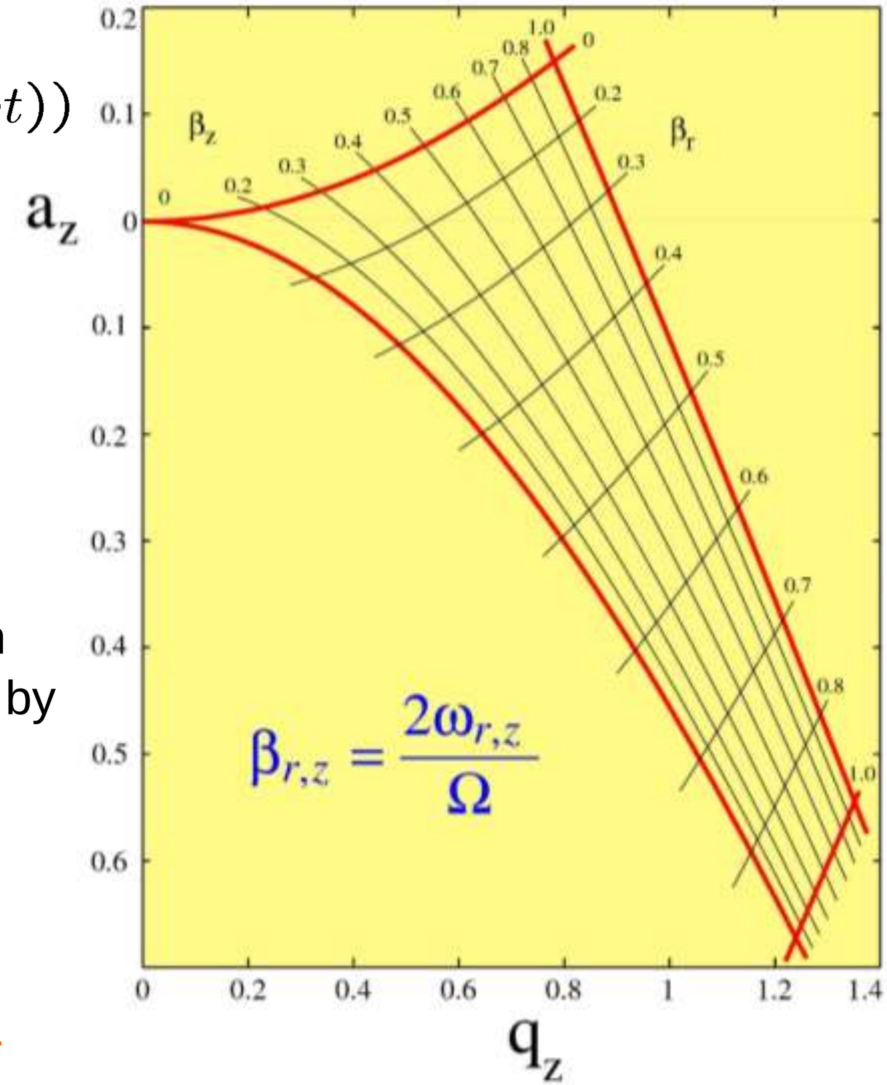

PP approx. : RMP 75, 281 (2003), NJP 14, 093023 (2012), PRL 109, 263003 (2012)

Real 3-Dim. Paul traps

ideal 3-Dim. Paul trap with equi-potental surfaces formed by copper electrodes

quadrupole trap from Mainz

ideal surfaces:

$$r^2 - 2z^2 = \pm\, r_0^2$$

endcap electrodes at distance

$$r_0/z_0 = \sqrt{2}$$

but non-ideal surfaces do trap also well:

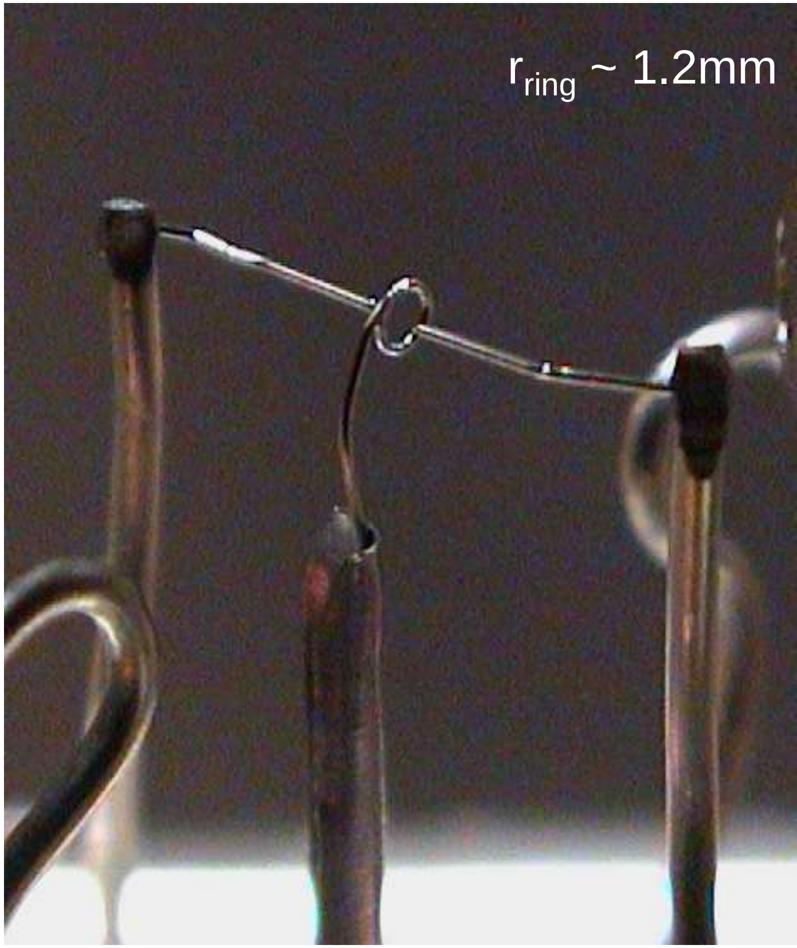

A. Mundt, Innsbruck

Real 3-Dim. Paul traps

ideal 3 dim. Paul trap with equi-potential surfaces formed by copper electrodes

Fig. 6 quadrupole trap from Mainz

non-ideal surfaces

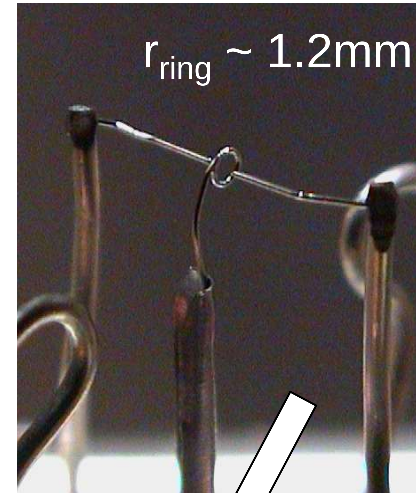

RMP 82, 2609 (2010)

numerical calculation of equipotential lines

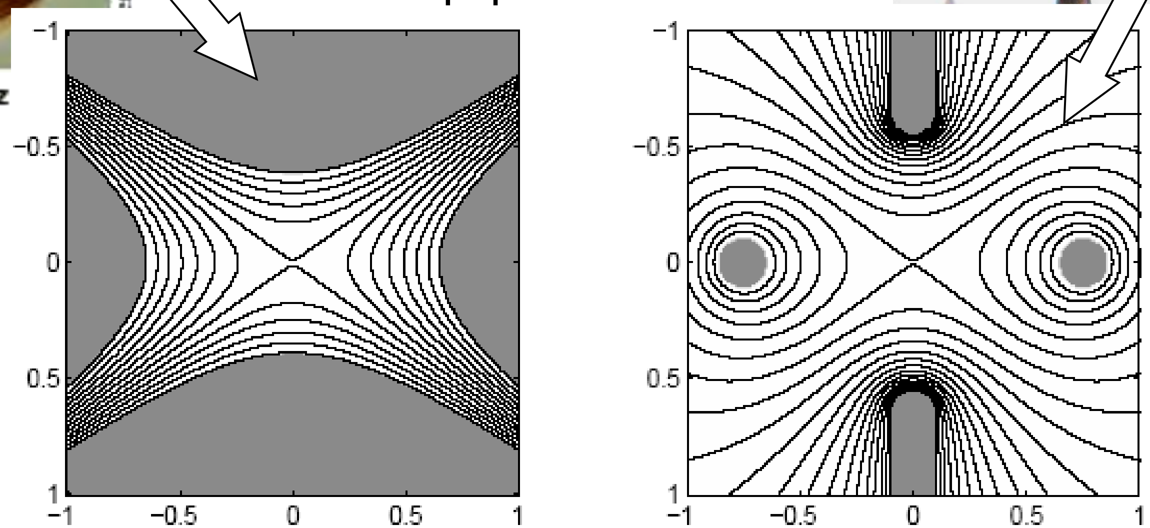

Equipotential lines of a quadrupole potential (left plot) and an approximate quadrupole potential (right). Both potentials have a cylindrical symmetry. The horizontal axis corresponds to the radial direction, the vertical axis is the symmetry axis. The electrode structure shown in the right plot is the one used for the experiments if length is measured in millimeters. It is composed of a ring electrode and two cylindrical electrodes with hemispheric endcaps.

similar potential near the center

2-Dim. Paul mass filter stability diagram

time depending potential $$\Phi(x,y,t) = \Phi_0(t) \cdot (x^2 - y^2)$$

with $$\Phi_0(t) = (U + V cos(\Omega_{RF} t))/r_0^2$$

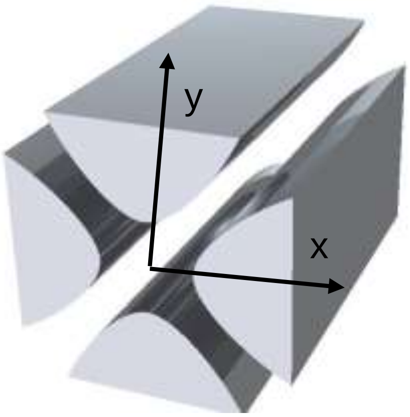

dynamical confinement in the x- y-plane

$$\boxed{\begin{aligned} &\ddot{x} + (a - 2\ q\ cos(2\tau))x = 0 \\ &\ddot{y} - (a - 2\ q\ cos(2\tau))y = 0 \end{aligned}}$$

with substitutions

$$a_i = -\frac{4QU}{mr_0^2\Omega_{RF}^2} \qquad q_i = -\frac{2QV}{mr_0^2\Omega_{RF}^2} \qquad \tau = \frac{1}{2}\Omega_{RF} t$$

radial trap radius r_0

2-Dim. Paul mass filter stability diagram

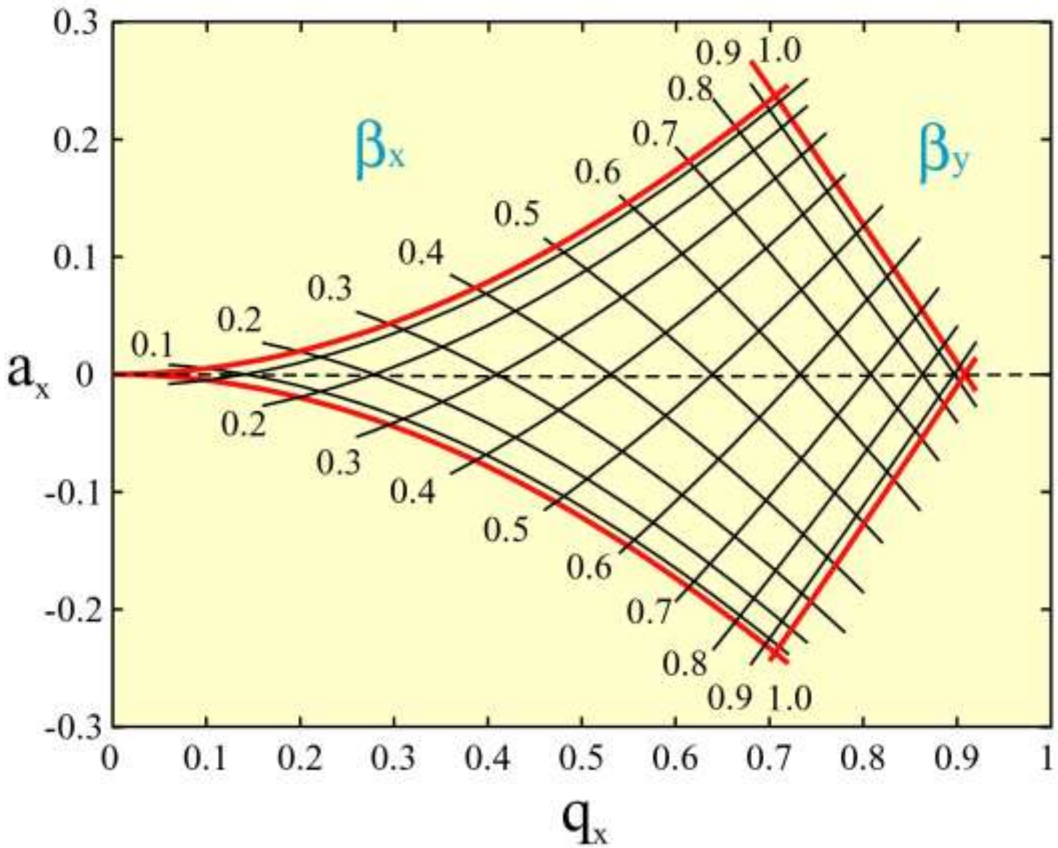

$$\omega_i = \beta_i \frac{\Omega_{RF}}{2}$$

$$\beta_i = \sqrt{a_i + \frac{q_i}{2}}$$

$$a_i = -\frac{4QU}{mr_0^2\Omega_{RF}^2} \qquad q_i = -\frac{2QV}{mr_0^2\Omega_{RF}^2} \qquad i = x, y$$

A Linear Paul trap

plug the ends of a mass filter by positive electrodes:

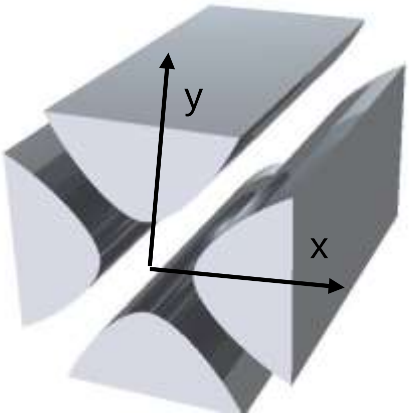

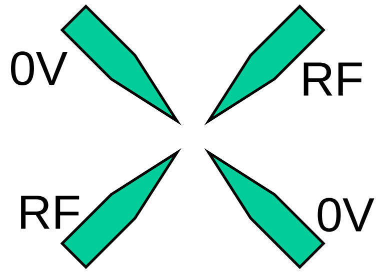

mass filter blade design

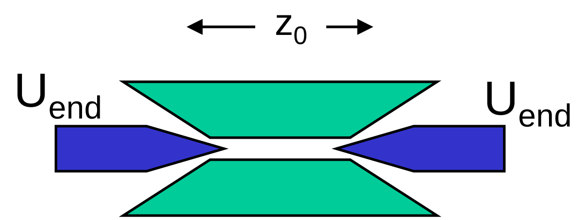

side view

numerically calculate the axial electric potential,
fit parabula into the potential
and get the axial trap frequency

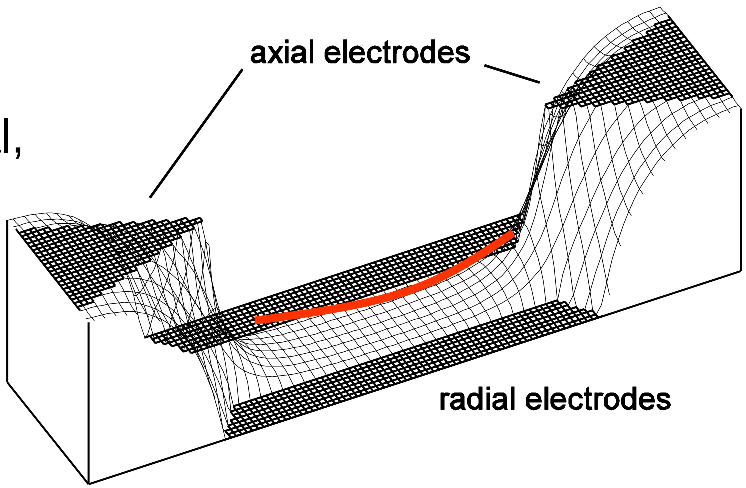

$$\boxed{\omega_z = \sqrt{\frac{2\kappa Q U_{end}}{m z_0}}}$$

with k geometry factor

Numerical tools: RMP 82, 2609 (2010)

Innsbruck design of linear ion trap

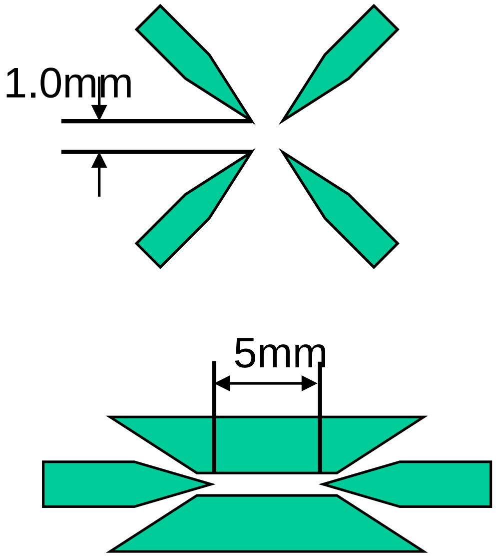

Blade design

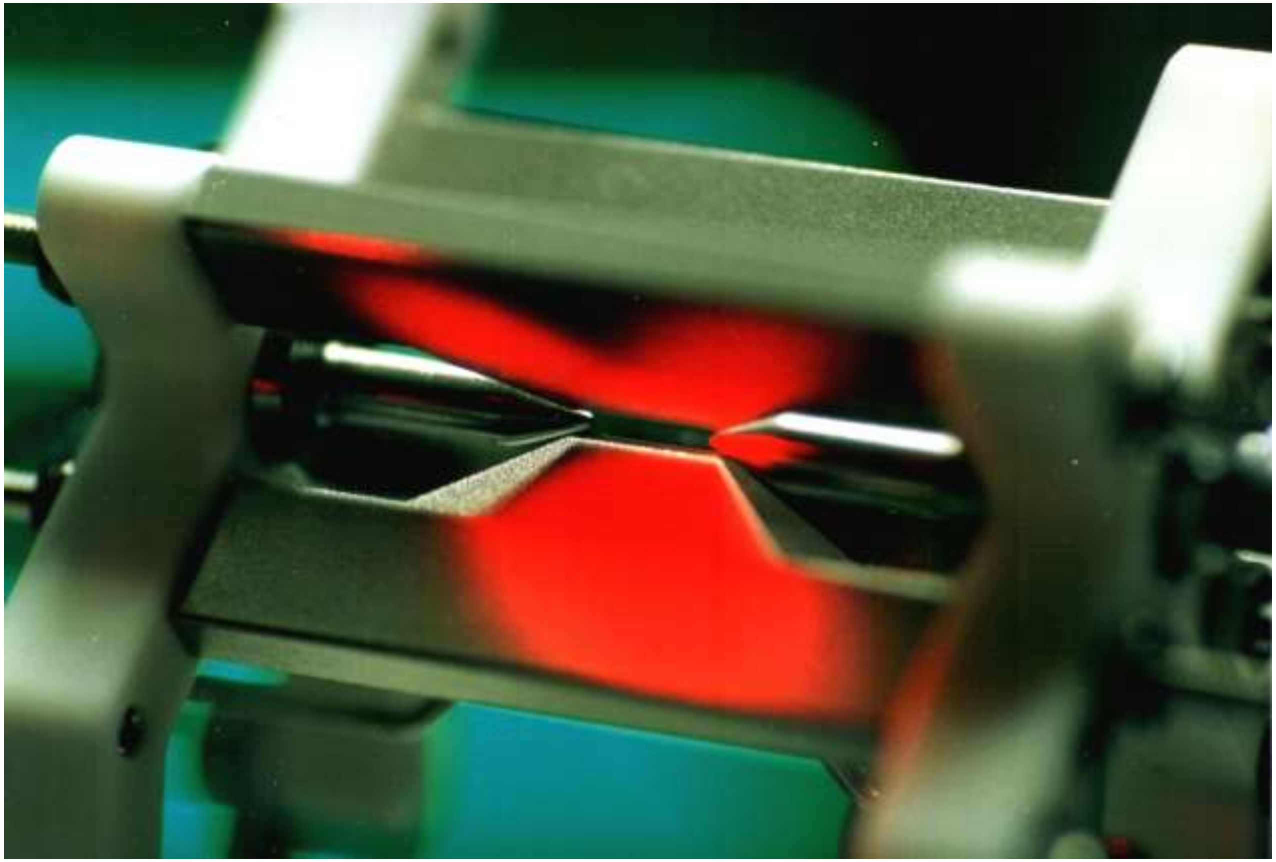

$\omega_{axial} \approx 0.7 - 2\ \mathrm{MHz}$ $\omega_{radial} \approx 5\ \mathrm{MHz}$

$$trap\ depth \approx eV$$

F. Schmidt-Kaler, et al., Appl. Phys. B 77, 789 (2003).

Ion crystals:
Equilibrium positions and eigenmodes

Equilibrium positions in the axial potential

$$V = \sum_{m=1}^{N} \frac{1}{2} M\nu^2 x_m(t)^2 + \sum_{\substack{n,m=1\\ m\neq n}}^{N} \frac{Z^2e^2}{8\pi\epsilon_0} \frac{1}{|x_n(t) - x_m(t)|},$$

trap potential mutual ion repulsion

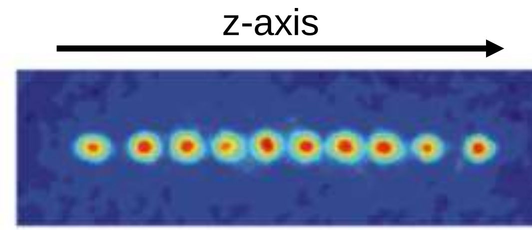

find equilibrium positions x^0: $x_m(t) \approx x_m^{(0)} + q_m(t)$ ions oscillate with *q(t)* arround

condition for equilibrium: $\left(\partial V / \partial x_m\right)_{x_m = x_m^{(0)}} = 0$

dimensionless positions $u_m = x_m^{(0)}/l$ with length scale $l^3 = \frac{Z^2e^2}{4\pi\epsilon_0 M\omega_{ax}^2}$

$^{40}Ca^{+} at\ 1MHz \rightarrow 4.5\mu m$

$$\longrightarrow \quad u_m - \sum_{n=1}^{m-1} \frac{1}{(u_m - u_n)^2} + \sum_{n=m+1}^{N} \frac{1}{(u_m - u_n)^2} = 0$$

$$(m = 1, 2, \ldots N).$$

D. James, Appl. Phys. B 66, 181 (1998)

Equilibrium positions in the axial potential

$$u_m - \sum_{n=1}^{m-1} \frac{1}{(u_m - u_n)^2} + \sum_{n=m+1}^{N} \frac{1}{(u_m - u_n)^2} = 0$$

$$(m = 1, 2, \ldots N) .$$

set of N equations for u_m

force of the trap potential

Coulomb force of all ions from left side

Coulomb force of all ions from left side

numerical solution (Mathematica), e.g. *N=5* ions

```
(* N=5  *)
Clear[a, a1, a2, a3, a4, a5, a6, a7, a8, a9, a10]
[lösche
a = Table[{a1, a2, a3, a4, a5, a6, a7, a8, a9, a10}, ];
 [Tabelle
equ5 = Table[a[[m]]
          [Tabelle
   - Sum[1 / (a[[m]] - a[[n]])^2, {n, 1, m - 1}]
     [summiere
   + Sum[1 / (a[[m]] - a[[n]])^2, {n, m + 1, 5}], {m, 1, 5}]
     [summiere
aa5 = Timing[FindRoot[equ5, {a1, -10}, {a2, -1}, {a3, 0.1}, {a4, 1}, {a5, 10}]]
        [Dauer   [ermittle Nullstelle
```

$$\Big\{a1 + \frac{1}{(a1-a2)^2} + \frac{1}{(a1-a3)^2} + \frac{1}{(a1-a4)^2} + \frac{1}{(a1-a5)^2},\ a2 - \frac{1}{(-a1+a2)^2} + \frac{1}{(a2-a3)^2} + \frac{1}{(a2-a4)^2} + \frac{1}{(a2-a5)^2},\ a3 - \frac{1}{(-a1+a3)^2} - \frac{1}{(-a2+a3)^2} + \frac{1}{(a3-a4)^2} + \frac{1}{(a3-a5)^2},$$
$$a4 - \frac{1}{(-a1+a4)^2} - \frac{1}{(-a2+a4)^2} - \frac{1}{(-a3+a4)^2} + \frac{1}{(a4-a5)^2},\ a5 - \frac{1}{(-a1+a5)^2} - \frac{1}{(-a2+a5)^2} - \frac{1}{(-a3+a5)^2} - \frac{1}{(-a4+a5)^2}\Big\}$$

```
{0.01 Second, {a1 -> -1.7429, a2 -> -0.822101, a3 -> 1.2717 × 10^-17, a4 -> 0.822101, a5 -> 1.7429}}

aa5[[2]][[2]][[2]]
-0.822101

abs5 = Table[aa5[[2]][[i]][[2]], {i, 1, 5}]
          [Tabelle
{-1.7429, -0.822101, 1.2717 × 10^-17, 0.822101, 1.7429}
```

equilibrium positions	-1.74	-0.82	0	+0.82	+1.74

Linear crystal equilibrium positions

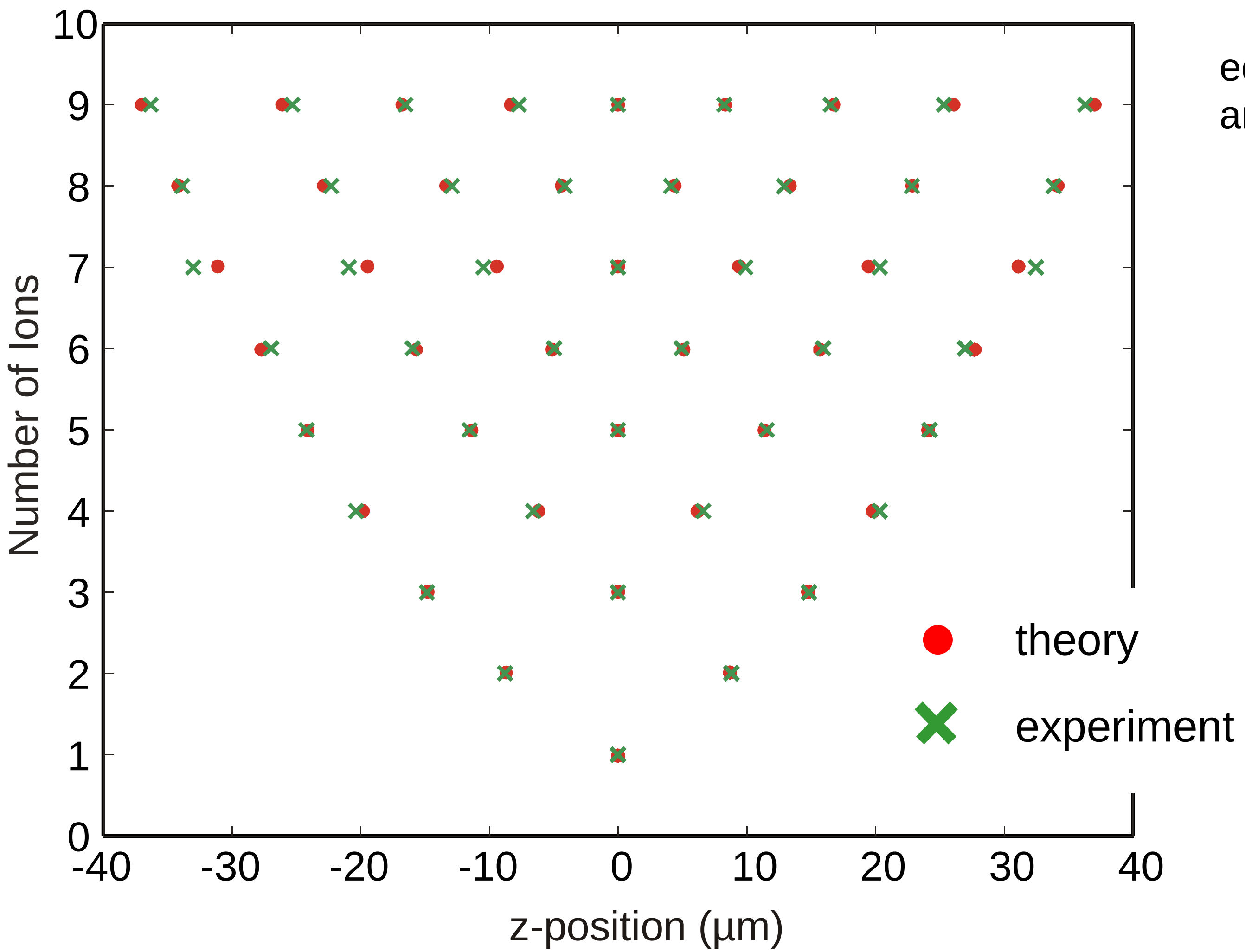

equilibrium positions
are not equally spaced

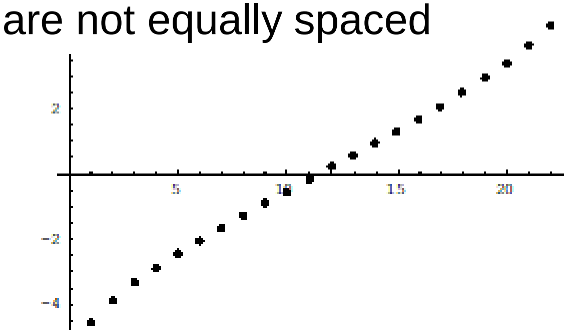

minimum inter-ion distance:

$$u_{min}(N) = \left(\frac{Z^2 e^2}{4\pi\epsilon_0 M\omega_{ax}}\right)\frac{2.018}{N^{0.559}}$$

H. C. Nägerl et al.,
Appl. Phys. B 66, 603 (1998)

Eigenmodes and Eigenfrequencies

Lagrangian of the axial ion motion: $L = T + V$

describes small excursions arround equilibrium positions

$$= \frac{M}{2}\sum_{m=1}^{N}(\dot{q}_m)^2 - \frac{1}{2}\sum_{m,n=1}^{N} q_n q_n \left(\frac{\partial^2 V}{\partial x_n \partial x_m}\right)_0 + \ldots$$

$$= \frac{M}{2}\left(\sum_{m=1}^{N} \dot{q}_m^2 - \omega_{ax}^2 \sum_{m,n=1}^{N} A_{nm} q_n q_n\right)$$

D. James, Appl. Phys. B 66, 181 (1998)

with $$A_{mn} = 1 + 2\sum_{\substack{n \neq m \\ n=0}}^{N} \frac{1}{|u_m - u_n|^3} \quad if \quad m = n$$

and $$A_{mn} = -\frac{2}{|u_m - u_n|^3} \quad if \quad m \neq n$$

linearized Coulomb interaction leads to Eigenmodes, but the next term in Tailor expansion leads to mode coupling, which is however very small.

C. Marquet, et al., Appl. Phys. B 76, 199 (2003)

Eigenmodes and Eigenfrequencies

numerical solution (Mathematica), e.g. *N=4* ions

```
(*      N=4      AXIAL         **************************)
A4 = Table[
      Tabelle
    If[m != n,
    wenn
     -2 / Abs[u4[[m]] - u4[[n]]]^3,
          Absolutwert
     1. + 2 Sum[ If[ i ≠ m, 1. / Abs[(u4[[m]] - u4[[i]])^3] , 0], {i, 1, 4}]  ],
           s···  wenn             Absolutwert
                                        {m, 1, 4}, {n, 1, 4}];
```

Matrix, to diagonize

```
TableForm[Eigenvectors[A4]]
Tabellendar··  Eigenvektoren
freq4 = Sqrt[Eigenvalues[A4]]   (* Modenfrequenzen *)
        Qua··  Eigenwerte
TableForm[A4];
Tabellendarstellung
```

-0.213213	0.674196	-0.674196	0.213213
0.5	-0.5	-0.5	0.5
-0.674196	-0.213213	0.213213	0.674196
-0.5	-0.5	-0.5	-0.5

{3.05096, 2.41039, 1.73205, 1.}

Eigenvectors pictorial

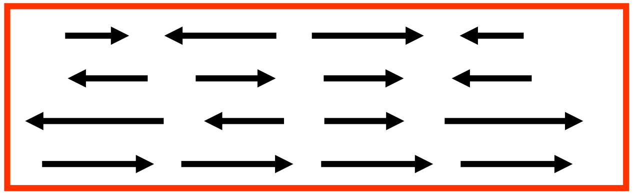

Eigenvalues

$$(3.059 \pm 0.008)\omega_{ax} \quad \sqrt{29/5}\omega_{ax} \quad \sqrt{3}\omega_{ax} \quad 1\omega_{ax}$$

depends on *N*   does not

for the radial modes: *Market et al., Appl. Phys. B76, (2003) 199*

Common mode excitations

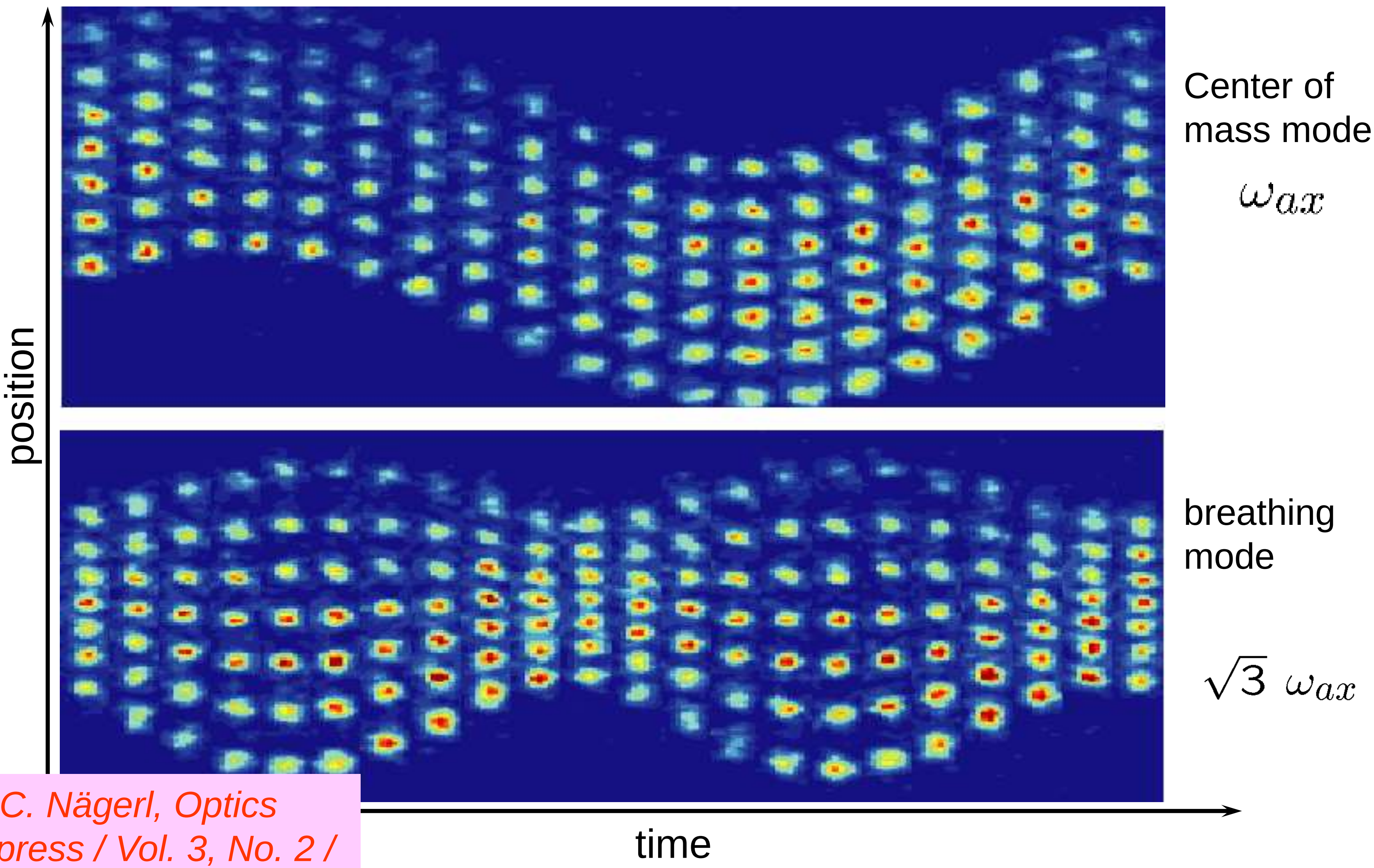

H. C. Nägerl, Optics Express / Vol. 3, No. 2 / 89 (1998).

Breathing mode excitation

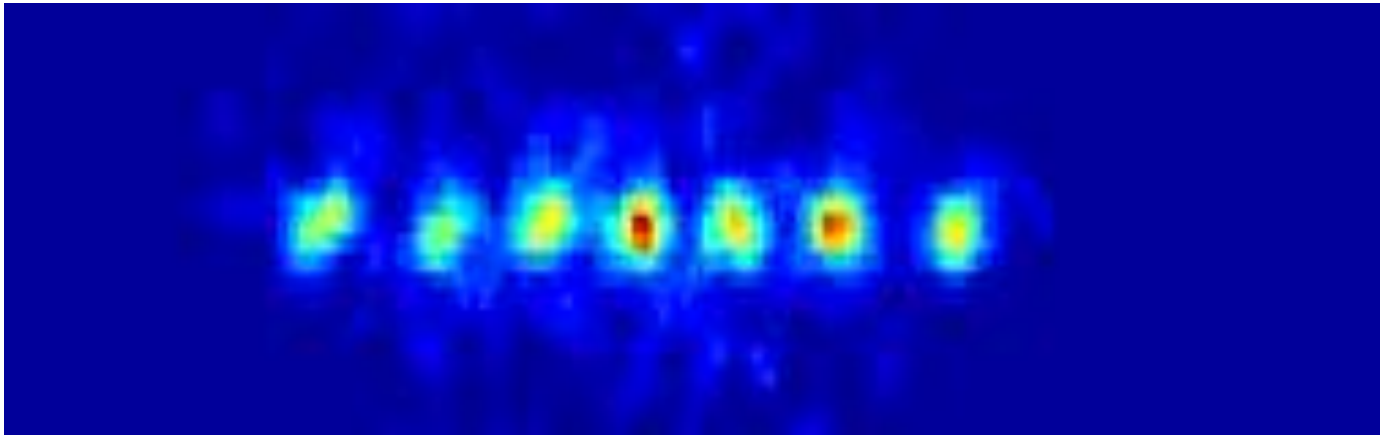

H. C. Nägerl, Optics Express / Vol. 3, No. 2 / 89 (1998).

1D, 2D, 3D ion crystals

Wineland et al., J. Res. Natl. Inst. Stand. Technol. 103, 259 (1998)

Enzer et al., PRL85, 2466 (2000)

- Depends on $\alpha=(\omega_{ax}/\omega_{rad})^2$
- Depends on the number of ions $a_{crit}= cN^{\beta}$

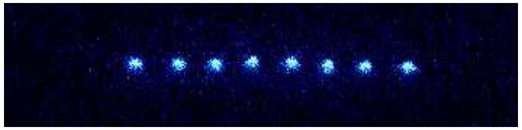

1D

- Generate a planar Zig-Zag when $\omega_{ax} < \omega^{y}_{rad} << \omega^{x}_{rad}$
- Tune radial frequencies in y and x direction

Planar crystal equilibrium positions

2D

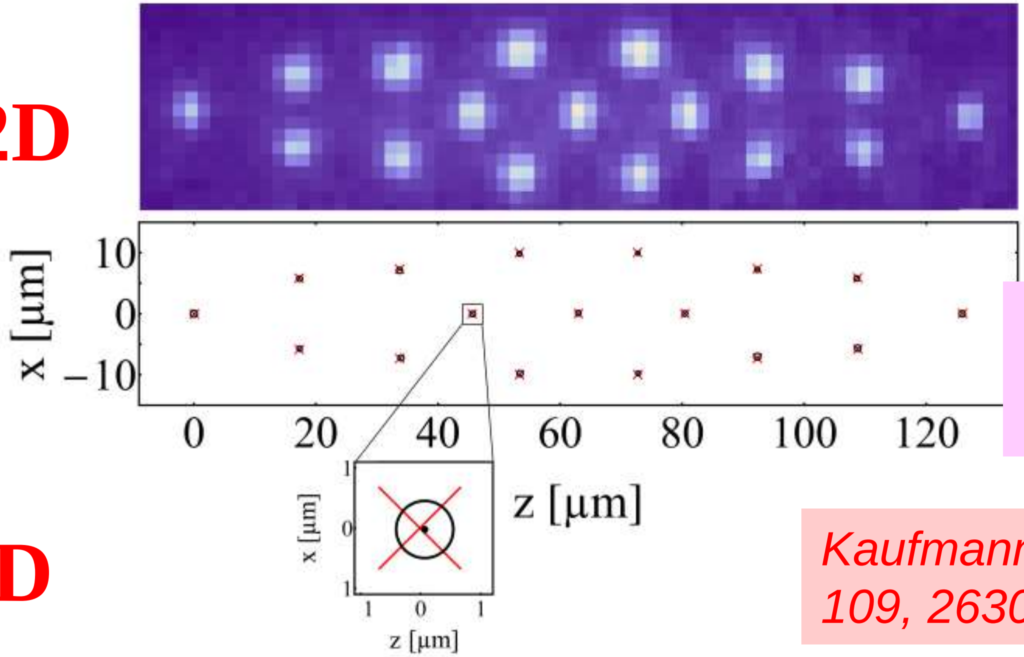

δx~50nm ±0.25%

Kaufmann et al, PRL 109, 263003 (2012)

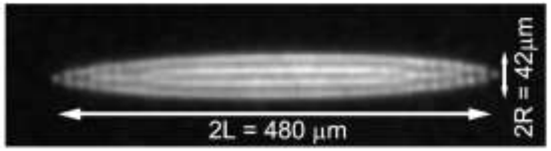

3D

There are many structural phase transitions!

- Vary anisotropy and observe the critcal α_i
- Agreement with expected values

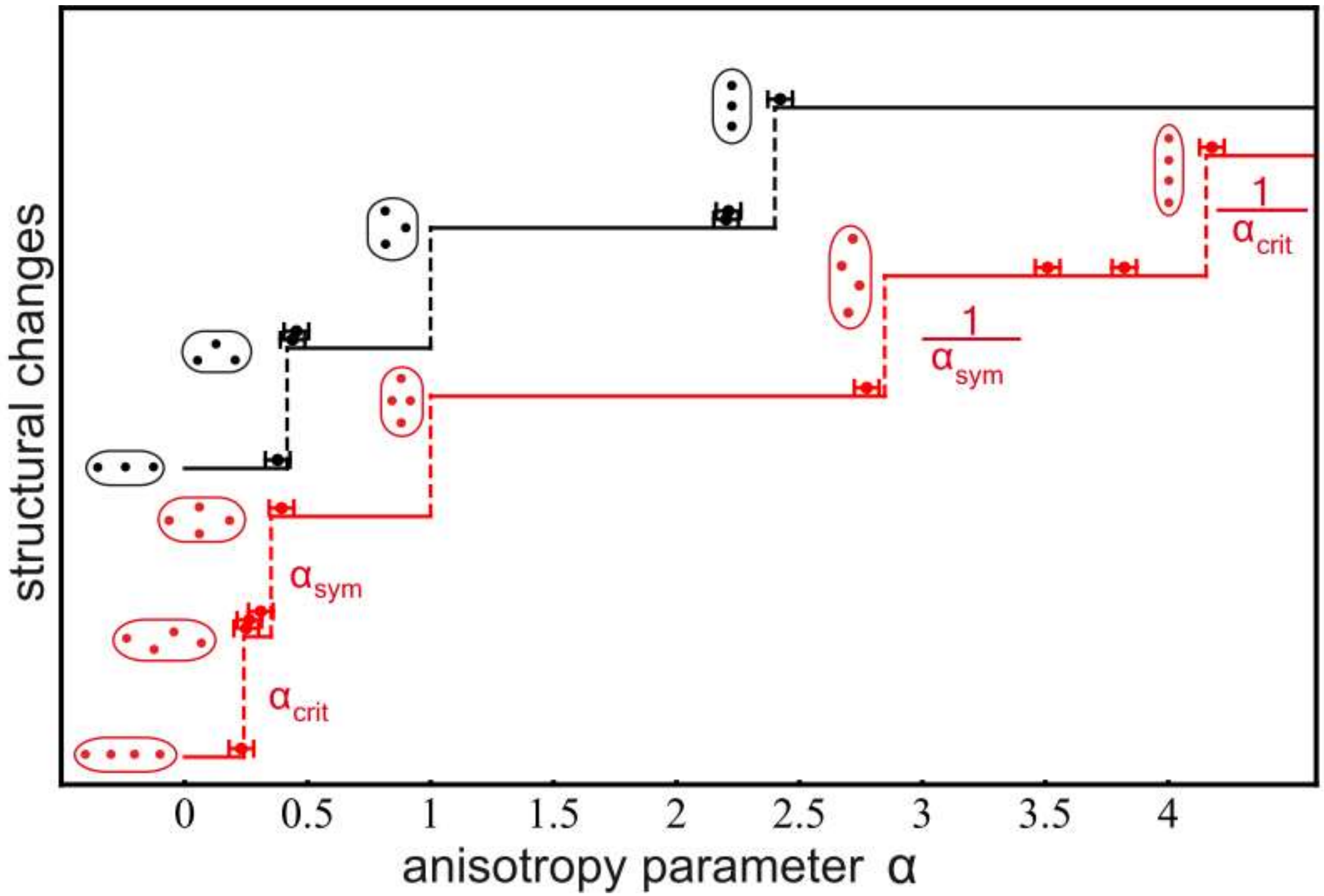

Structural phase transition in ion crystal

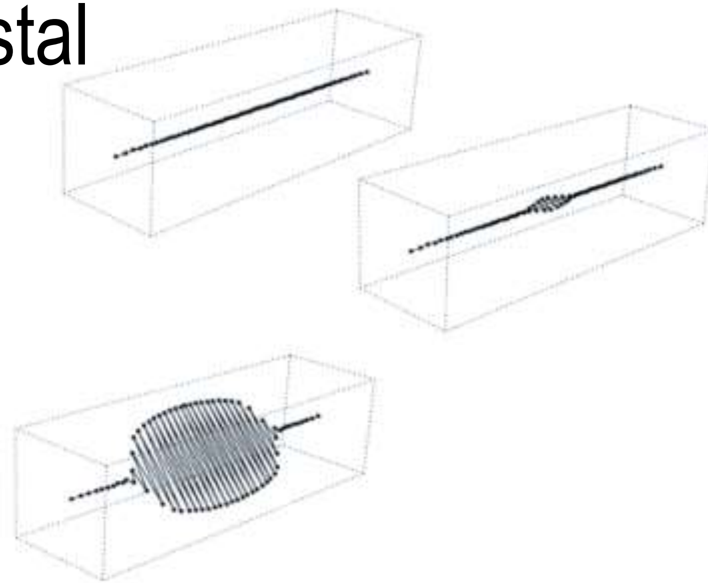

$$H = \sum_{i,\mu}\left(\frac{p_{i\mu}^2}{2m} + \frac{1}{2}m\omega_\mu^2 r_{i\mu}^2\right) + \frac{1}{2}\sum_{i\neq j}\frac{e^2}{4\pi\varepsilon_0}\frac{1}{|\mathbf{r}_i - \mathbf{r}_j|}$$

E_{kin} $\quad$ $U_{pot,harm.}$ $\quad$ $U_{Coulomb}$

$$H \approx H_0 = \hbar\omega_z \sum_n \sqrt{\gamma_n^x}a_n^\dagger a_n + \sqrt{\gamma_n^y}b_n^\dagger b_n + \sqrt{\lambda_n^z}c_n^\dagger c_n$$

Phase transition @ CP:

- One mode frequency → 0
- Large non-harmonic contributions
- coupled Eigen-functions
- Eigen-vectors reorder to generate new structures

6 ion crystal

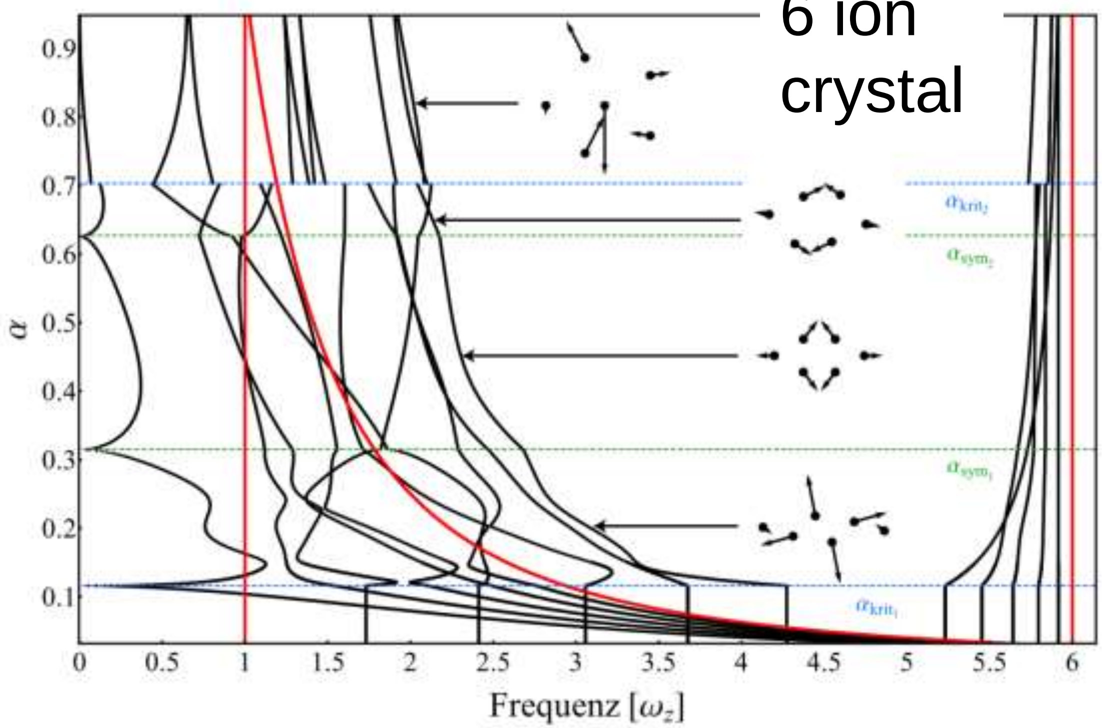

Ion crystal beyond harmonic approximations

$$H = \sum_{i,\mu}\left(\frac{p_{i\mu}^2}{2m} + \frac{1}{2}m\omega_\mu^2 r_{i\mu}^2\right) + \frac{1}{2}\sum_{i\neq j}\frac{e^2}{4\pi\varepsilon_0}\frac{1}{|\mathbf{r}_i - \mathbf{r}_j|}$$

E_{kin} $U_{pot,harm.}$ $U_{Coulomb}$

Marquet, Schmidt-Kaler, James, Appl. Phys. B 76, 199 (2003)

$$H^{(3)} = 3\frac{z_0}{4l_z}\hbar\omega_z\sum_{n,m,p}\frac{D_{nmp}^{(3)}}{\sqrt[4]{\gamma_n^x\gamma_m^x\lambda_p^z}}(a_n + a_n^\dagger)(a_m + a_m^\dagger)(c_p + c_p^\dagger)$$

$$H^{(4)} = 3\left(\frac{z_0}{4l_z}\right)^2\hbar\omega_z\sum_{n,m,p,q}D_{nmpq}^{(4)}\frac{(a_n + a_n^\dagger)(a_m + a_m^\dagger)}{\sqrt[4]{\gamma_n^x\gamma_m^x}}\left[\frac{(a_p + a_p^\dagger)(a_q + a_q^\dagger)}{\sqrt[4]{\gamma_p^x\gamma_q^x}} + \frac{2(b_p + b_p^\dagger)(b_q + b_q^\dagger)}{\sqrt[4]{\gamma_p^y\gamma_q^y}} - \frac{8(c_p + c_p^\dagger)(c_q + c_q^\dagger)}{\sqrt[4]{\lambda_p^z\lambda_q^z}}\right].$$

Z_0 wavepaket size

l_z ion distance

γ,λ ion frequencies

$D_{n,m,p}$ coupling matrix

Non-linear couplings in ion crystal

Lemmer, Cormick, C. Schmiegelow, Schmidt-Kaler, Plenio, PRL 114, 073001 (2015)

$$H_{\mathrm{eff}}^{(4)} = H_{\mathrm{s}} + H_{\mathrm{d}}$$

$$H_{\mathrm{s}} = \hbar \frac{\Omega_{\mathrm{SI}}}{2} (a_{\mathrm{zz}}^{\dagger})^2 a_{\mathrm{zz}}^2 + \hbar \Delta\omega_{\mathrm{zz}} a_{\mathrm{zz}}^{\dagger} a_{\mathrm{zz}}$$

Self-interaction

$$H_{\mathrm{d}} = a_{\mathrm{zz}}^{\dagger} a_{\mathrm{zz}} \left(\hbar \Omega_{\mathrm{d},2}^{x} a_2^{\dagger} a_2 + \hbar \sum_{n=2,3} \Omega_{\mathrm{d,n}}^{y} b_n^{\dagger} b_n + \Omega_{\mathrm{d,n}}^{z} c_n^{\dagger} c_n \right)$$

Cross Kerr coupling

$$H_{\mathrm{res}}^{(3)} = \hbar \Omega_{\mathrm{T}} [a_{\mathrm{zz}}^2 c_{\mathrm{str}}^{\dagger} + (a_{\mathrm{zz}}^{\dagger})^2 c_{\mathrm{str}}]$$

Resonant inter-mode coupling

…. remind yourself of non-linear optics: frequency doubling, Kerr effect, self-phase modulation, ….

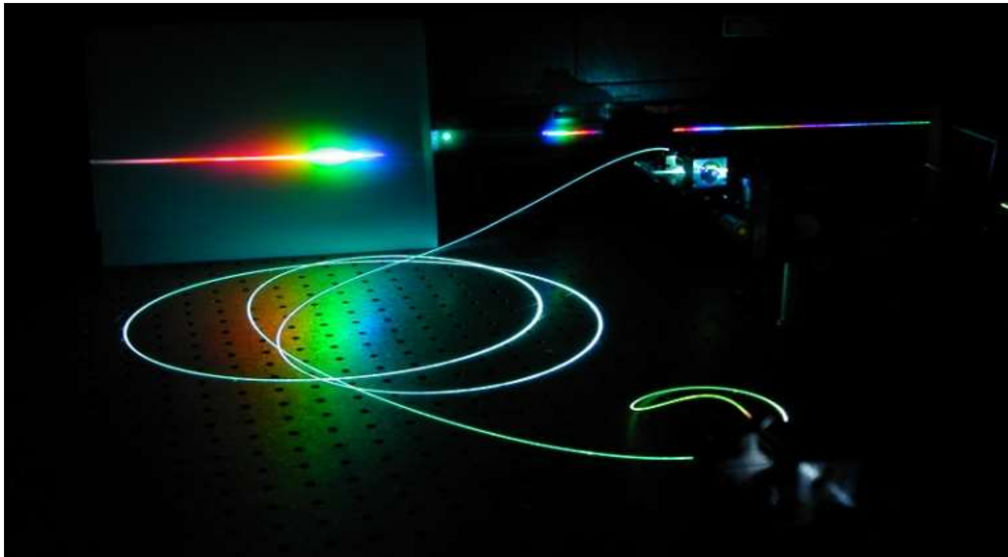

Non-linear couplings in ion crystal

Ding, et al, PRL119, 193602 (2017)

Cross
Kerr coupling

$$H_{\mathrm{d}} = a^{\dagger}_{\mathrm{zz}} a_{\mathrm{zz}} \left(\hbar \Omega^{x}_{\mathrm{d},2} a^{\dagger}_{2} a_{2} + \hbar \sum_{n=2,3} \Omega^{y}_{\mathrm{d,n}} b^{\dagger}_{n} b_{n} + \Omega^{z}_{\mathrm{d,n}} c^{\dagger}_{n} c_{n} \right)$$

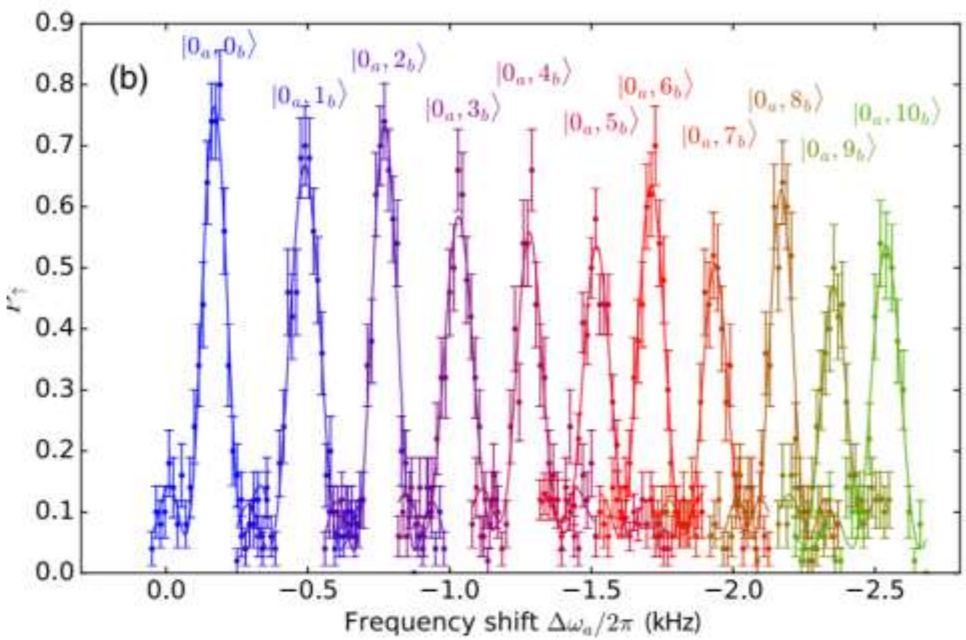

Resonant inter-mode coupling

$$H^{(3)}_{\mathrm{res}} = \hbar \Omega_{\mathrm{T}} [a^{2}_{\mathrm{zz}} c^{\dagger}_{\mathrm{str}} + (a^{\dagger}_{\mathrm{zz}})^{2} c_{\mathrm{str}}]$$

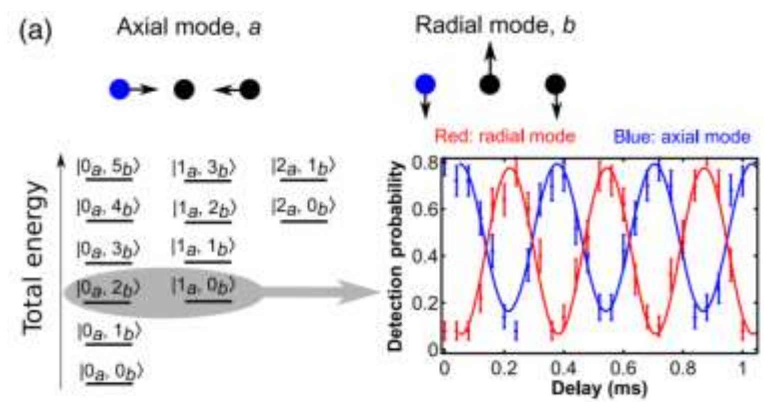

Micro-motion

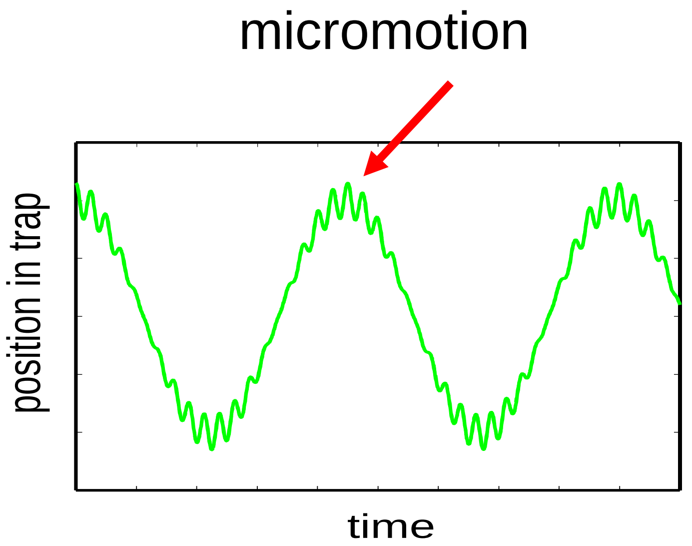

Problems due to micro-motion:

- relativistic Doppler shift in frequency measurements
- less scattered photons due to broader resonance line
- imperfect Doppler cooling due to line broadening
- AC Stark shift of the clock transition due to trap drive field Ω
- for larger # of ions: mutual coupling of ions can lead to coupling of secular frequency ω and drive frequency Ω.
- Heating of the ion motion
- for planar ion crystals non-equal excitation
- Shift of motional frequencies
- for atom-ion experiments, large collision energies

Kaufmann et al, PRL 109, 263003 (2012)

Feldker, et al, PRL 115, 173001 (2015)
Ewald et al, PRL122, 253401 (2019)

Micro-motion

frequency Ω : Micro-motion
Ion is shaken with the RF drive frequency

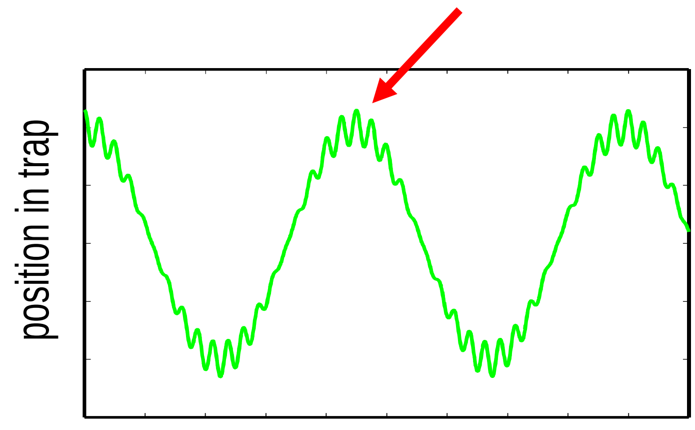

alters the optical spectrum of the trapped ion due to Doppler shift, Bessel functions *$J_n(b)$* appear.
Electric field seen by the ion:

$$E = \sum J_n(\beta) e^{-in\Omega t}$$

PRL 81, 3631 (1998), PRA 60, R3335 (1999)

a) broadening of the ion's resonance

Wide line limit $\quad \gamma >> \Omega$

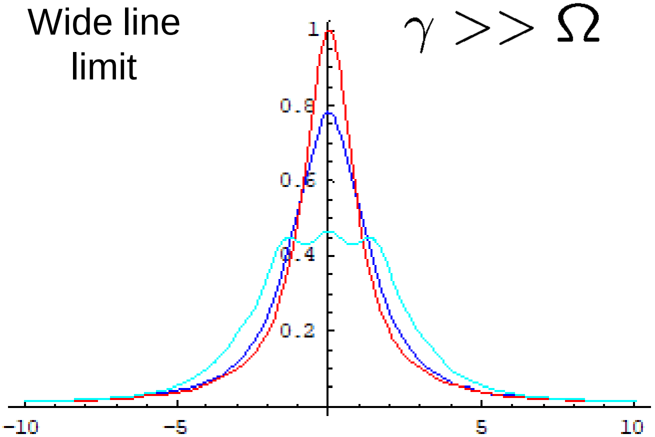

b) appearing of micro-motion sidebands

Narrow line limit $\quad \gamma << \Omega$

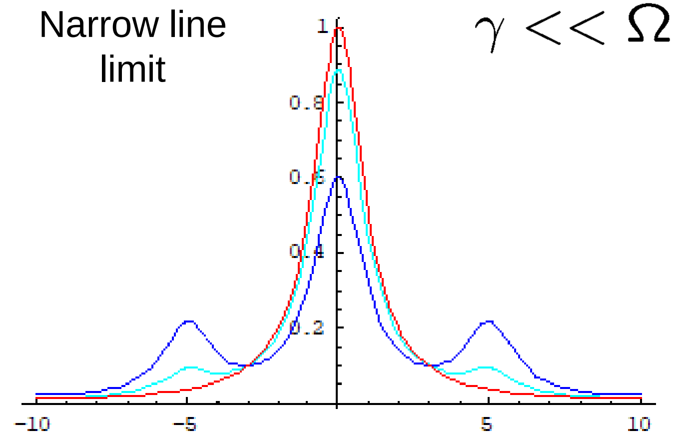

Compensate micro-motion

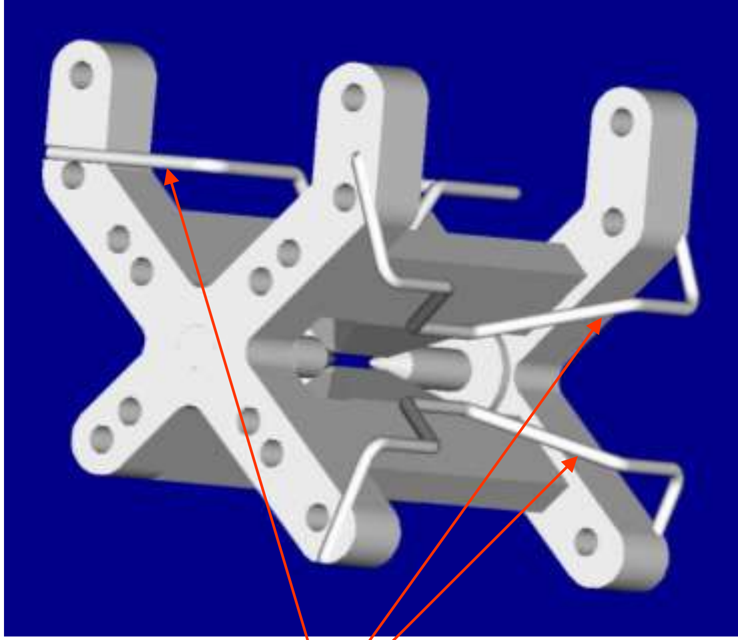

how to detect micro-motion:

a) detect the Doppler shift
and Doppler broadening

→ Fluorescence modulation technique:

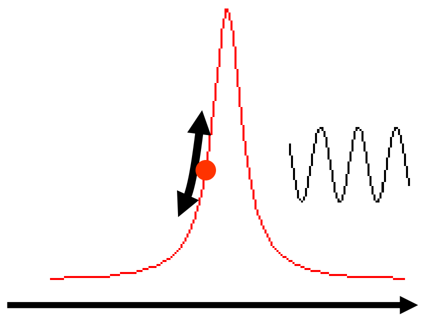

ion oscillation leads a modulation in # of scattered photons. Synchron detection via a START (photon) STOP (W_{RF} trigger) measurement

apply voltages here
and shift the ion into the symetry center
of the linear quadrupole

J. Appl. Phys. 83, 5025

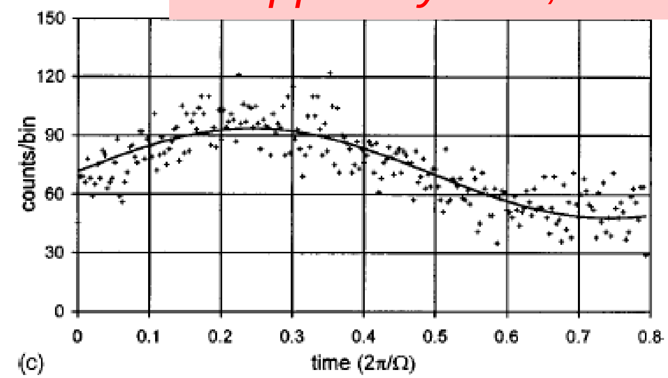

FIG. 4. Experimental fluorescence modulation signals for beam 1 of Fig. 3, using eight ions in the linear trap (points) and fit (solid line). Displacement of the ions from the trap axis along $(\hat{x}+\hat{y})/\sqrt{2}$ is (a) $0.9\pm0.3\ \mu\text{m}$, (b) $6.7\pm0.4\ \mu\text{m}$, and (c) $-6.7\pm0.4\ \mu\text{m}$.

b) detect micro-motional sidebands

→ Sideband spectroscopy

Laser cooling

Laser-ion interaction

  Lamb Dicke parameter
  Strong and weak
  confinement regime

Rate equation model
Cooling rate and cooling limit
Doppler cooling of ions

Resolved sideband spectroscopy

Reaching the ground state of vibration

Temperature measurement techniques

  Sideband Rabi oscillations
  Red / blue sideband ratio
  Carrier Rabi oscillations
  dark resonances
  observation of scatter light in far field

Basics: Harmonic oscillator

Why? The trap confinement is leads to three independend harmonic oscillators !

$$E = E_{kin} + E_{pot} = \frac{\vec{p}^2}{2m} + \frac{m}{2}\omega_{ax}^2 x^2$$

here only for the linear direction of the linear trap $\longrightarrow$ no micro-motion

treat the oscillator quantum mechanically and introduce *a*+ and *a*

$$x = \sqrt{\frac{\hbar}{2m\omega_{ax}}}(a + a^\dagger) \qquad p_x = i\sqrt{\frac{\hbar m \omega_{ax}}{2}}(a^\dagger - a)$$

and get Hamiltonian

$$\boxed{H_{oscillator} = \hbar\omega_{ax}(a^\dagger a + \frac{1}{2})}$$

Eigenstates |*n*> with:

$$H|n\rangle = \hbar\omega_{ax}(n + \frac{1}{2})|n\rangle$$

$$a^\dagger|n\rangle = \sqrt{n}|n-1\rangle$$

$$a|n\rangle = \sqrt{n+1}|n+1\rangle$$

Harmonic oscillator wavefunctions

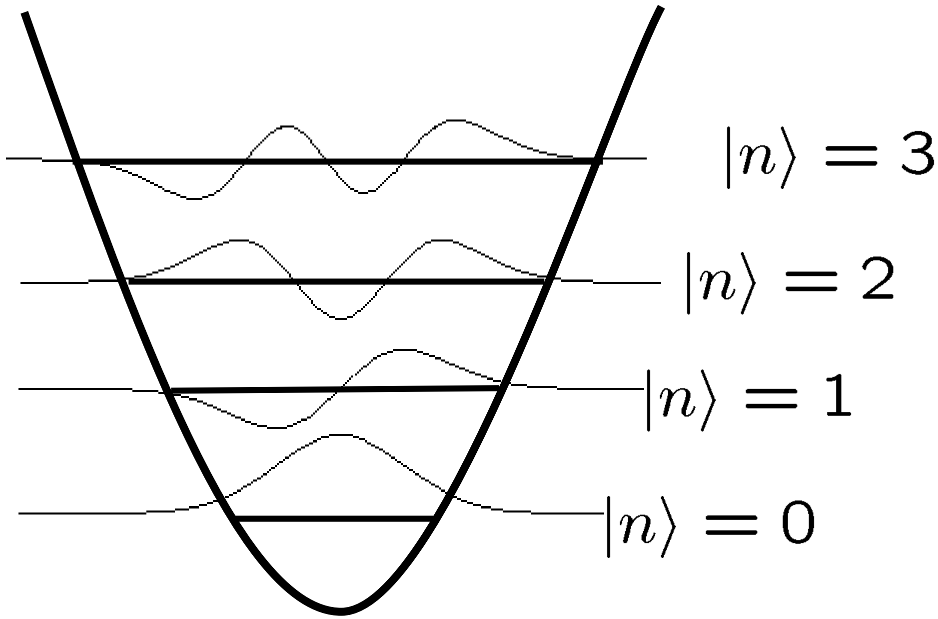

Eigen functions

$$u(x) \sim H(n,x)\, e^{-x^2}$$

with orthonormal Hermite polynoms
and energies:

$$E(n) = \hbar\omega_{ax}(n + \tfrac{1}{2})$$

Two – level atom

Why? Is an idealization which is a good approximation to real physical system in many cases

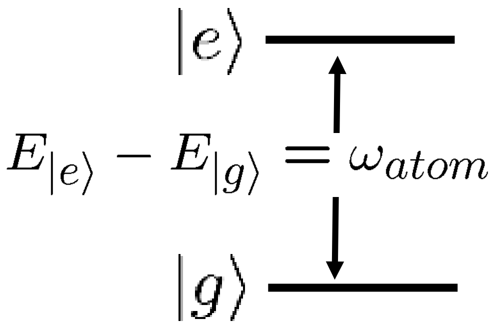

$$\boxed{\begin{aligned} H_{atom} &= \hbar\omega_{atom}(|e\rangle\langle e| - |g\rangle\langle g|) \\ &= \hbar\omega_{atom}\sigma_z \end{aligned}}$$

two level system is connected with spin ½ algebra using the Pauli matrices

$$\boxed{\begin{aligned} &|g\rangle\langle g| + |e\rangle\langle e| \rightarrow \hat{I} \\ &|g\rangle\langle e| + |e\rangle\langle g| \rightarrow \hat{\sigma_x} \\ &i(|g\rangle\langle e| - |e\rangle\langle g|) \rightarrow \hat{\sigma_y} \\ &|e\rangle\langle e| - |g\rangle\langle g| \rightarrow \hat{\sigma_z} \end{aligned}}$$

D. Leibfried, C. Monroe,
R. Blatt, D. Wineland,
Rev. Mod. Phys. 75, 281 (2003)

Two – level atom

Why? Is an idealization which is a good approximation to real pyhsical system in many cases

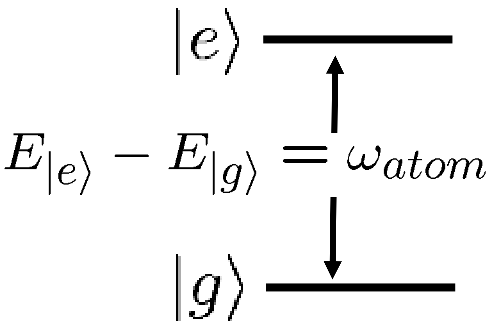

$$\boxed{\begin{aligned} H_{atom} &= \hbar\omega_{atom}(|e\rangle\langle e| - |g\rangle\langle g|) \\ &= \hbar\omega_{atom}\sigma_z \end{aligned}}$$

together with the harmonic oscillator leading to the ladder of eigenstates |g,n>, |e,n>:

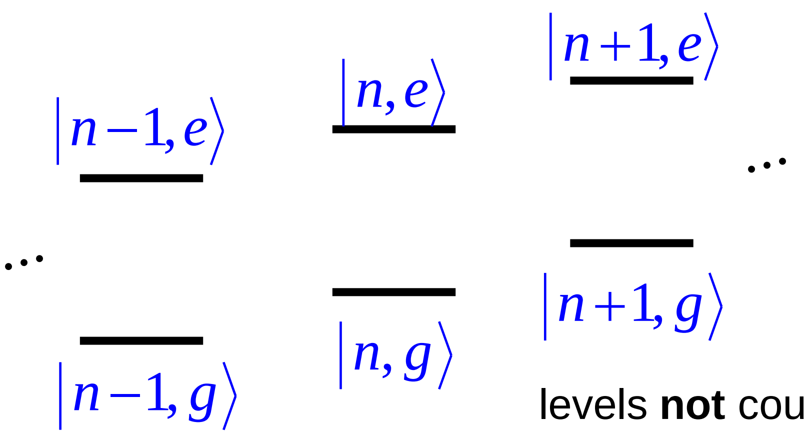

$$\boxed{H_0 = \frac{p^2}{2m_0} + \frac{1}{2}m_0\omega^2x^2 + \frac{1}{2}\hbar\omega_a\sigma_z}$$

levels **not** coupled

Laser coupling

dipole interaction, Laser radiation with frequency ω_l, and intensity $|E|^2$

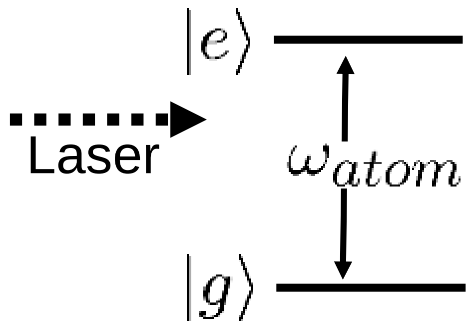

Rabi frequency: $\Omega_R = \langle g|\vec{d} \cdot \vec{E}|e\rangle$

$$\boxed{\begin{aligned} H_{ge} &= \hbar\frac{\Omega_R}{2}(|g\rangle\langle e| + |e\rangle\langle g|) \\ &= \hbar\frac{\Omega_R}{2}(\sigma^+ + \sigma^-) \end{aligned}}$$

with $\begin{aligned} |e\rangle\langle g| &\rightarrow \sigma^+ = (\sigma_x + i\sigma_y)/2 \\ |g\rangle\langle e| &\rightarrow \sigma^- = (\sigma_x - i\sigma_y)/2 \end{aligned}$

the laser interaction (running laser wave) has a spatial dependence:

$\vec{d} \cdot \vec{E} \longrightarrow \vec{d} \cdot \vec{E} e^{ikx}$ momentum kick, recoil: e^{ikx}

$$\boxed{\begin{aligned} H_{ge} &= \hbar\frac{\Omega_R}{2}(|g\rangle\langle e|e^{ikx} + |e\rangle\langle g|e^{-ikx}) \\ &= \tfrac{1}{2}\hbar\Omega(\sigma^+ + \sigma^-)(e^{i(kx-\omega_l t+\phi)} + e^{-i(kx-\omega_l t+\phi)}) \end{aligned}}$$

Laser coupling

in the rotating wave approximation

$$\boxed{H_{ge} = \frac{1}{2}\hbar\Omega(\sigma^{+} e^{i(\eta(a+a^{\dagger})} e^{-i\omega_l t} + \sigma^{-} e^{-i\eta(a+a^{\dagger})} e^{\omega_l t})}$$

using $x = \sqrt{\frac{\hbar}{2m\omega_{ax}}}(a + a^{\dagger})$

and defining the Lamb Dicke parameter η:

$$\boxed{\eta = k\sqrt{\frac{\hbar}{2m\omega_{ax}}}}$$

if the laser direction is at an angle ϕ to the vibration mode direction:

single photon transition

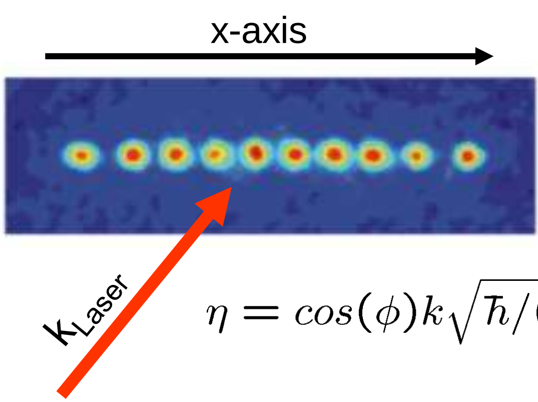

$\eta = cos(\phi)k\sqrt{\hbar/(2m\omega_{ax}}$

Raman transition: projection of $\Delta k = k_1 - k_2$

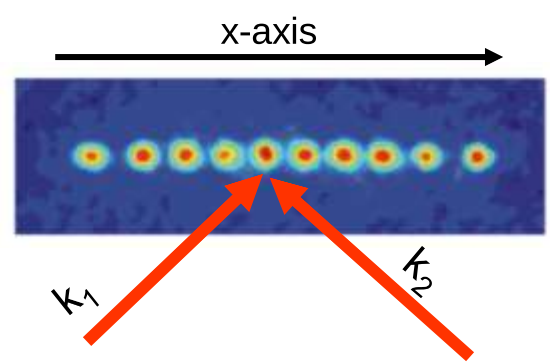

Interaction picture

$$H_{ge} = \frac{1}{2}\hbar\Omega(\sigma^{+} e^{i(\eta(a+a^{\dagger})} e^{-i\omega_l t} + \sigma^{-} e^{-i\eta(a+a^{\dagger})} e^{\omega_l t})$$

In the interaction picture defined by $U = e^{iHt/\hbar}$

we obtain for the Hamiltonian $H_I = U^{\dagger} H U$

$$\boxed{H_I = \frac{1}{2}\hbar\Omega\left(e^{i\eta(\hat{a}+\hat{a}^{\dagger})}\sigma^{+} e^{-i\Delta t} + e^{-i\eta(\hat{a}+\hat{a}^{\dagger})}\sigma^{-} e^{i\Delta t}\right)}$$

with $\hat{a} = a e^{i\omega t}, \Delta = \omega_{laser} - \omega_{atom}$ laser detuning Δ

coupling states $|g, n\rangle \leftrightarrow |e, n'\rangle$ with vibration quantum numbers n, n'

Laser coupling

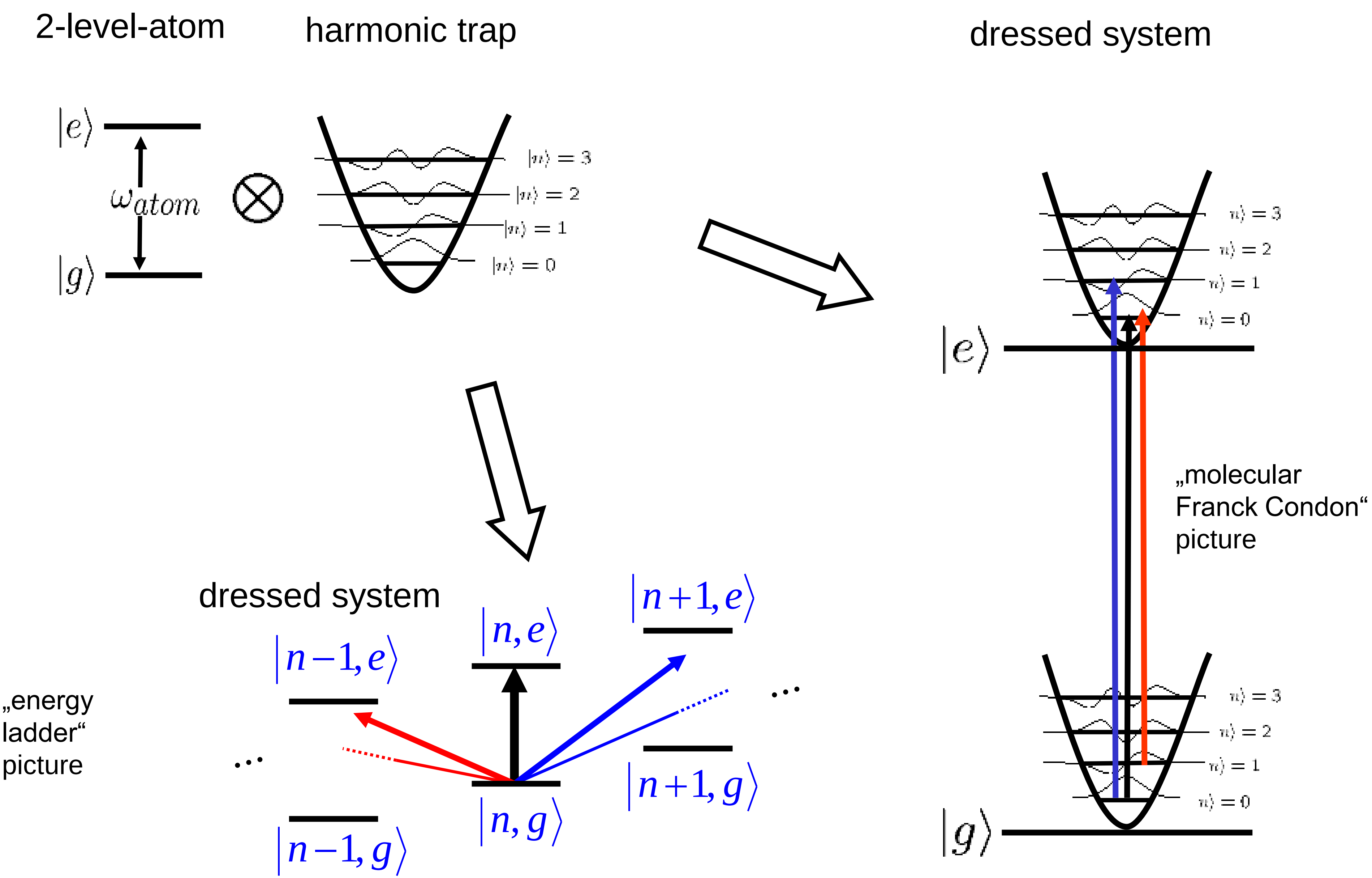

Lamb Dicke Regime

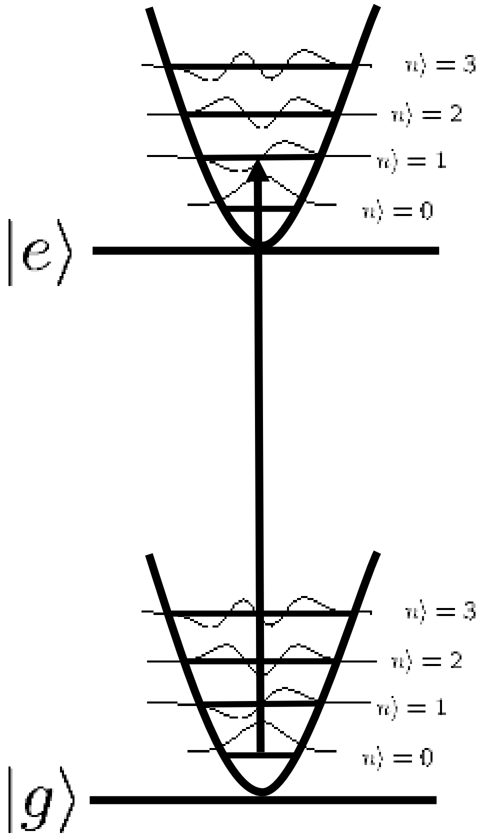

$$\langle g, n|\vec{d} \cdot \vec{E} e^{ikx}|e, m\rangle =$$

$$\langle g|\vec{d} \cdot \vec{E}|e\rangle \langle n|e^{ikx}|m\rangle =$$

$$\hbar \frac{\Omega_{Rabi}}{2} \langle n|e^{i\eta(a+a^\dagger)}|m\rangle \approx$$

$$\boxed{\eta^2(a + a^\dagger)^2 << 1 \longrightarrow \eta^2(2n+1) << 1}$$

$$\hbar \frac{\Omega_{Rabi}}{2} \langle n|1 + (i\eta(a + a^\dagger)|m\rangle =$$

$$\boxed{\hbar \frac{\Omega_{Rabi}}{2} \left(\delta_{n,m} + i\eta\sqrt{n}\,\delta_{m=n-1} + i\eta\sqrt{n+1}\,\delta_{m=n+1}\right)}$$

laser is tuned to the resonances:

carrier: $\Omega_{Rabi}\ (1 - \eta^2(2n+1))$

blue sideband: $\Omega_{Rabi}\ \eta\sqrt{n+1}$

red sideband: $\Omega_{Rabi}\ \eta\sqrt{n}$

Wavefunctions in momentum space

$$\eta = \sqrt{\frac{\hbar k}{2m\omega_{trap}}} = \sqrt{\frac{\omega_{recoil}}{\omega_{trap}}}$$

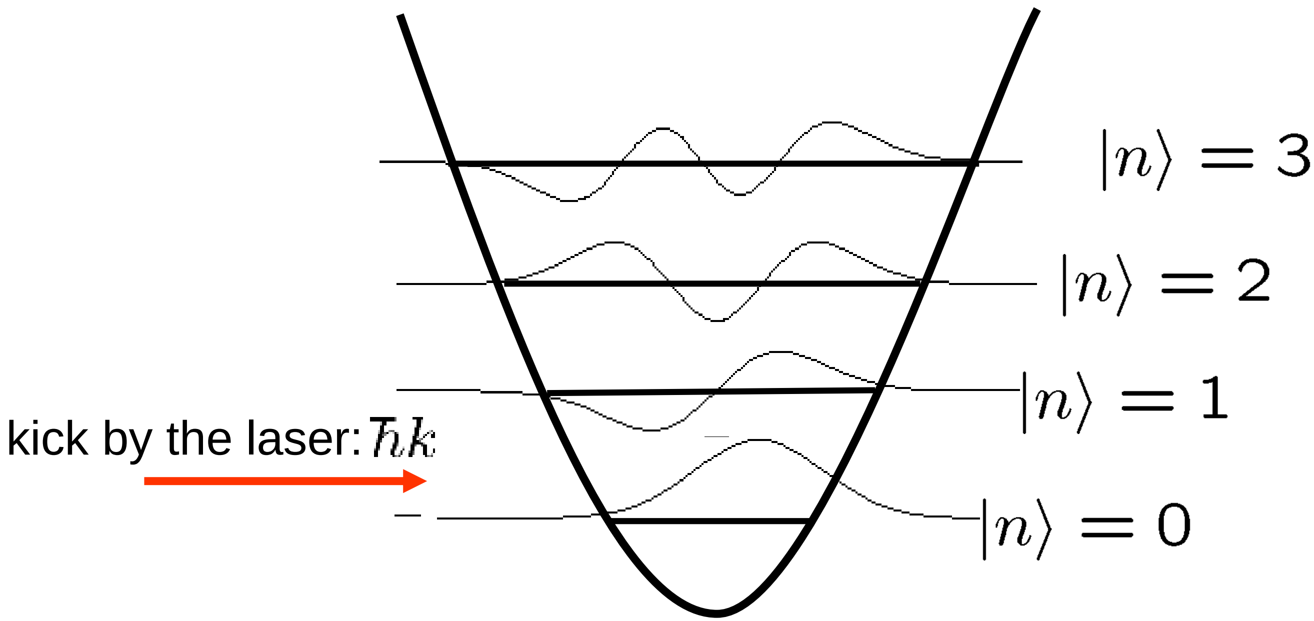

kicked wave function is **non-**orthogonal to the other wave functions

Experimental example

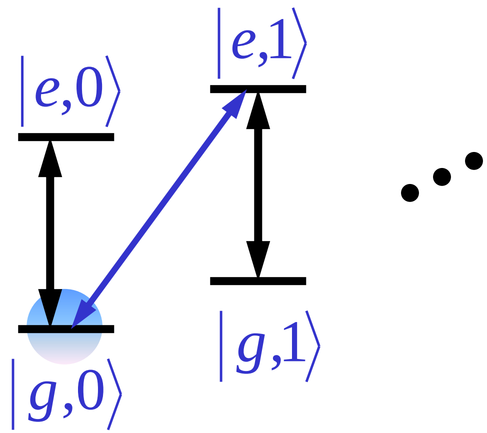

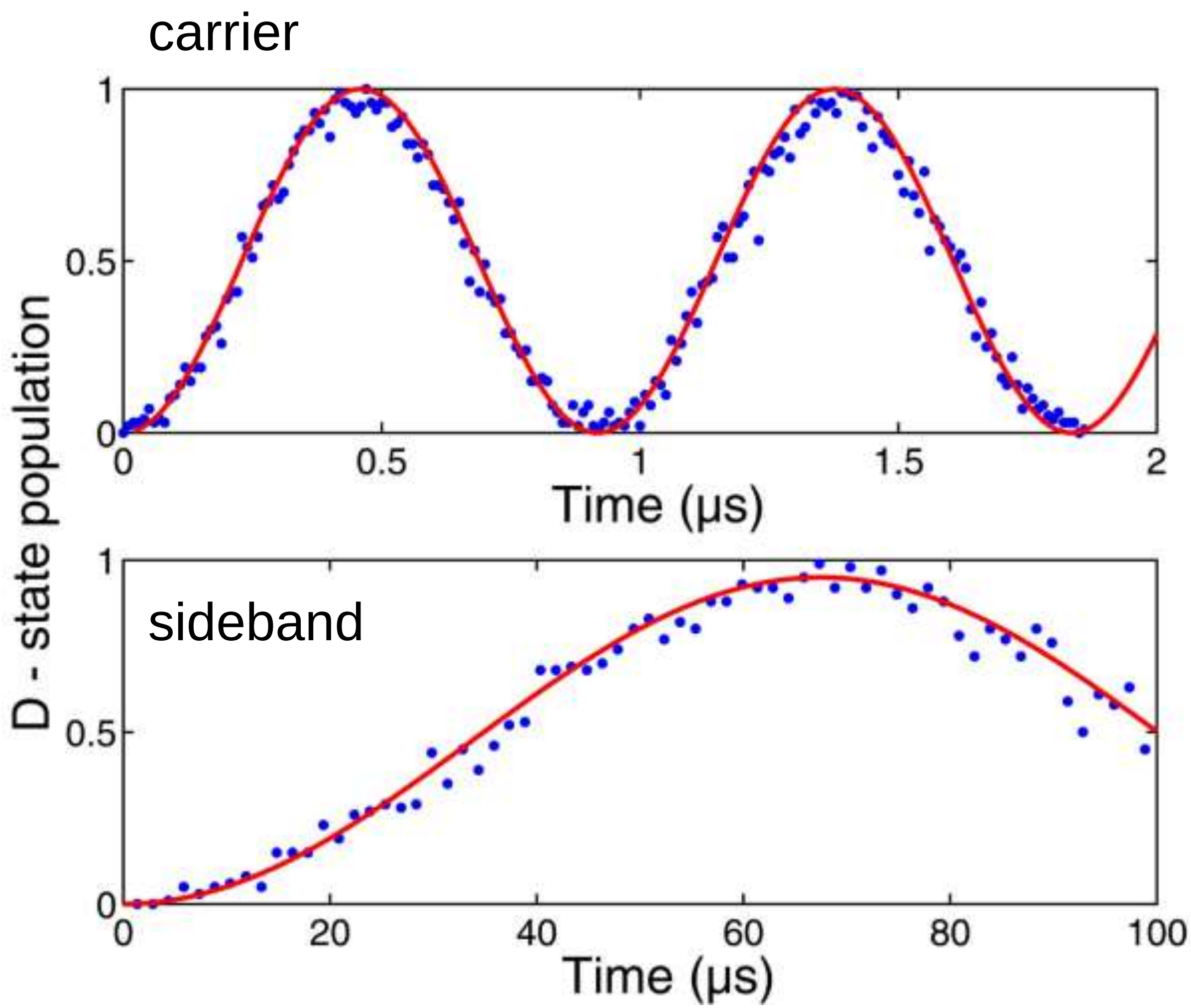

carrier and sideband
Rabi oscillations
with Rabi frequencies

Ω_{Rabi} and $\Omega_{Rabi}\ \eta$

Outside Lamb Dicke Regime

$$\hbar\frac{\Omega_{Rabi}}{2}\langle n|e^{i\eta(a+a^\dagger)}|m\rangle =$$

$$\boxed{e^{-(\eta^2/2)}\ \eta^{|m|}\ L_n^{|m|}(\eta^2)\ \left(\frac{n!}{(n+m)!}\right)^{sign(m)/2}}$$

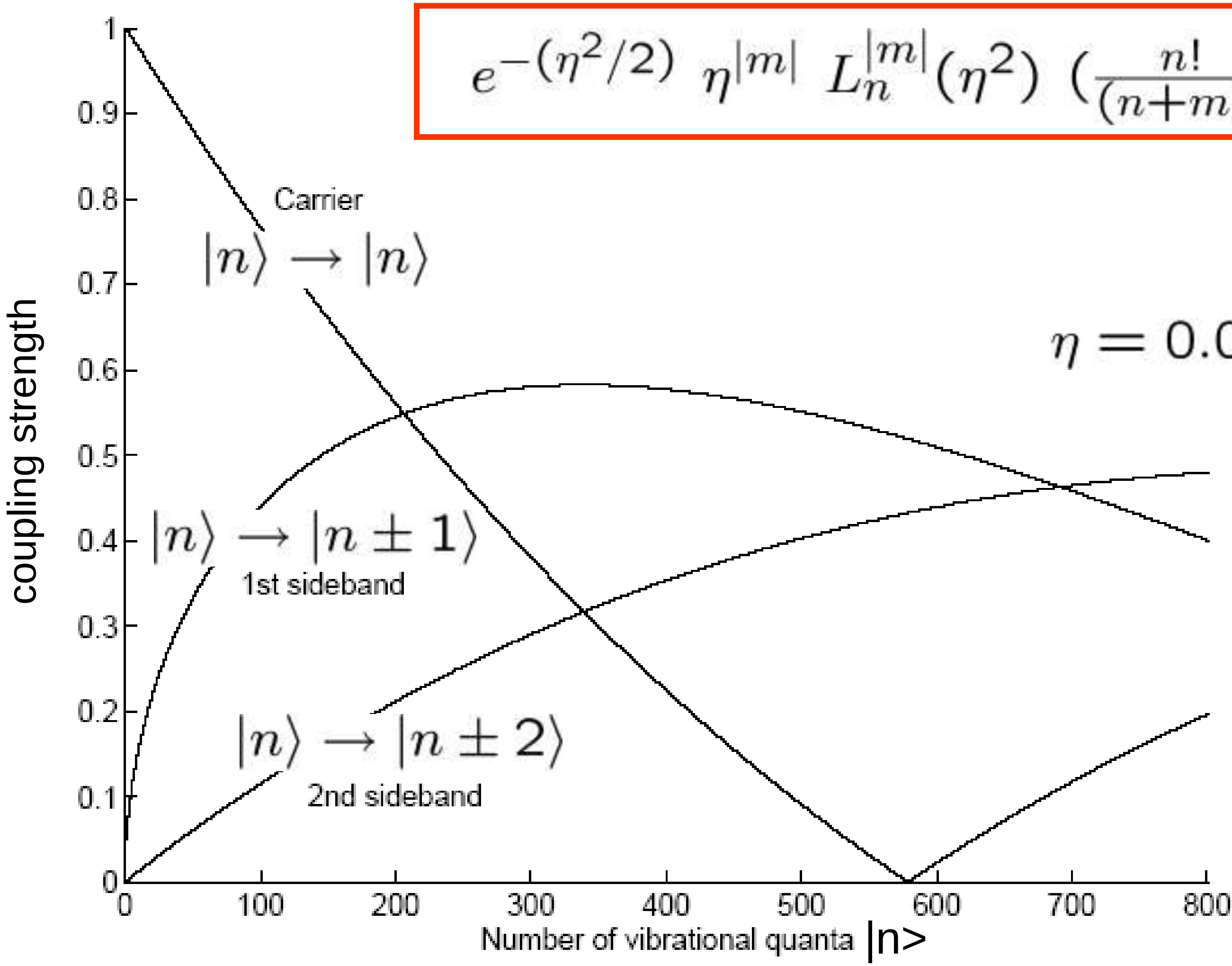

„Strong confinement“

$$\boxed{\omega_{trap} >> \gamma}$$

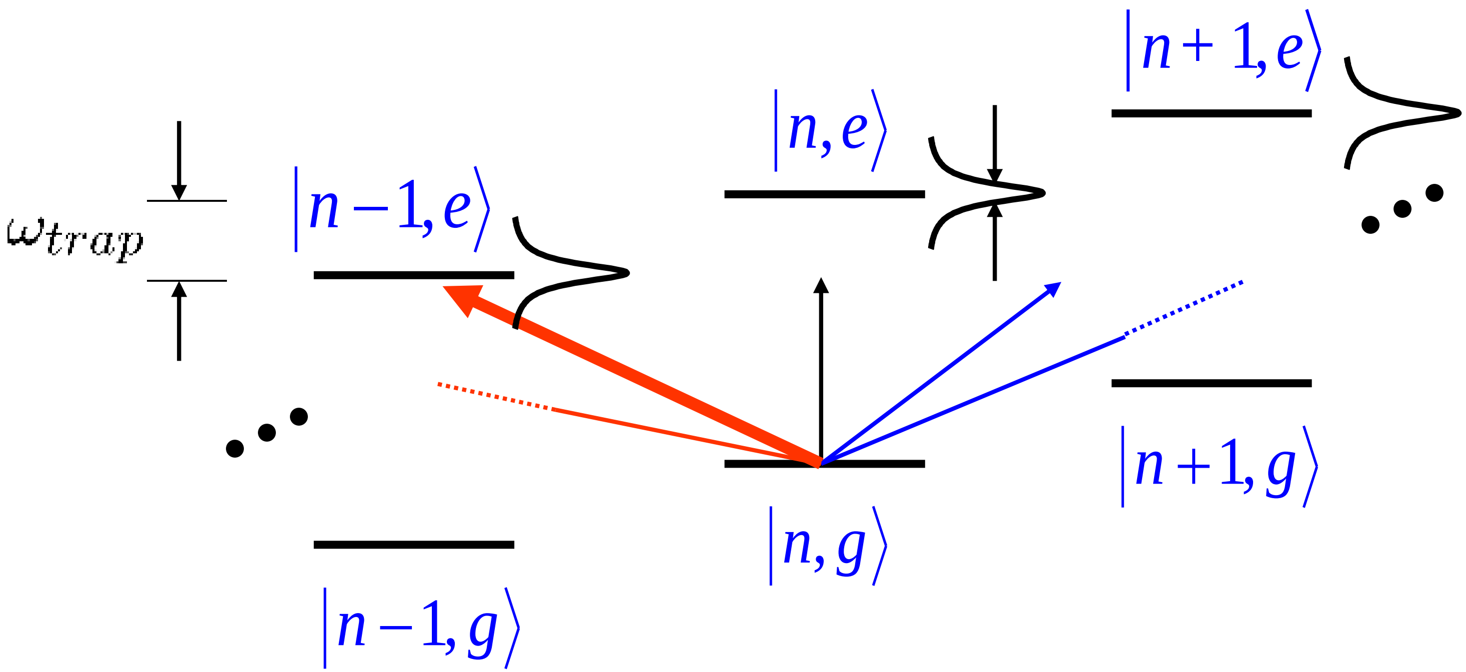

strong confinement – well resolved sidebands:
Selective excitation of a single sideband only,
e.g. here the red SB

„Weak confinement“

$$\boxed{\omega_{trap} << \gamma}$$

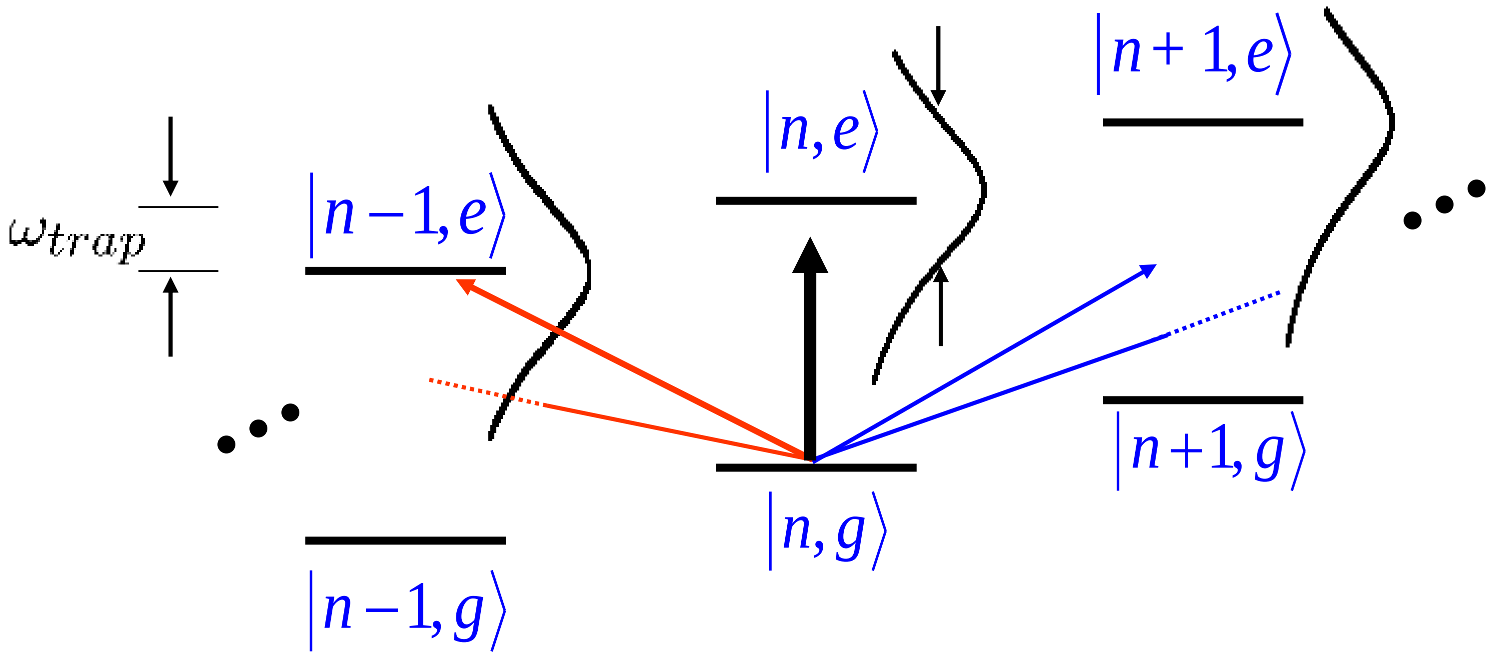

weak confinement:
Sidebands are not resolved on that transition.
Simultaneous excitation of several vibrational states

Two-level system dynamics

spont. decay rate γ

Rabi frequency Ω

incoherent: $\Omega < \gamma$

coherent: $\Omega > \gamma$

Solution of
optical Bloch equations

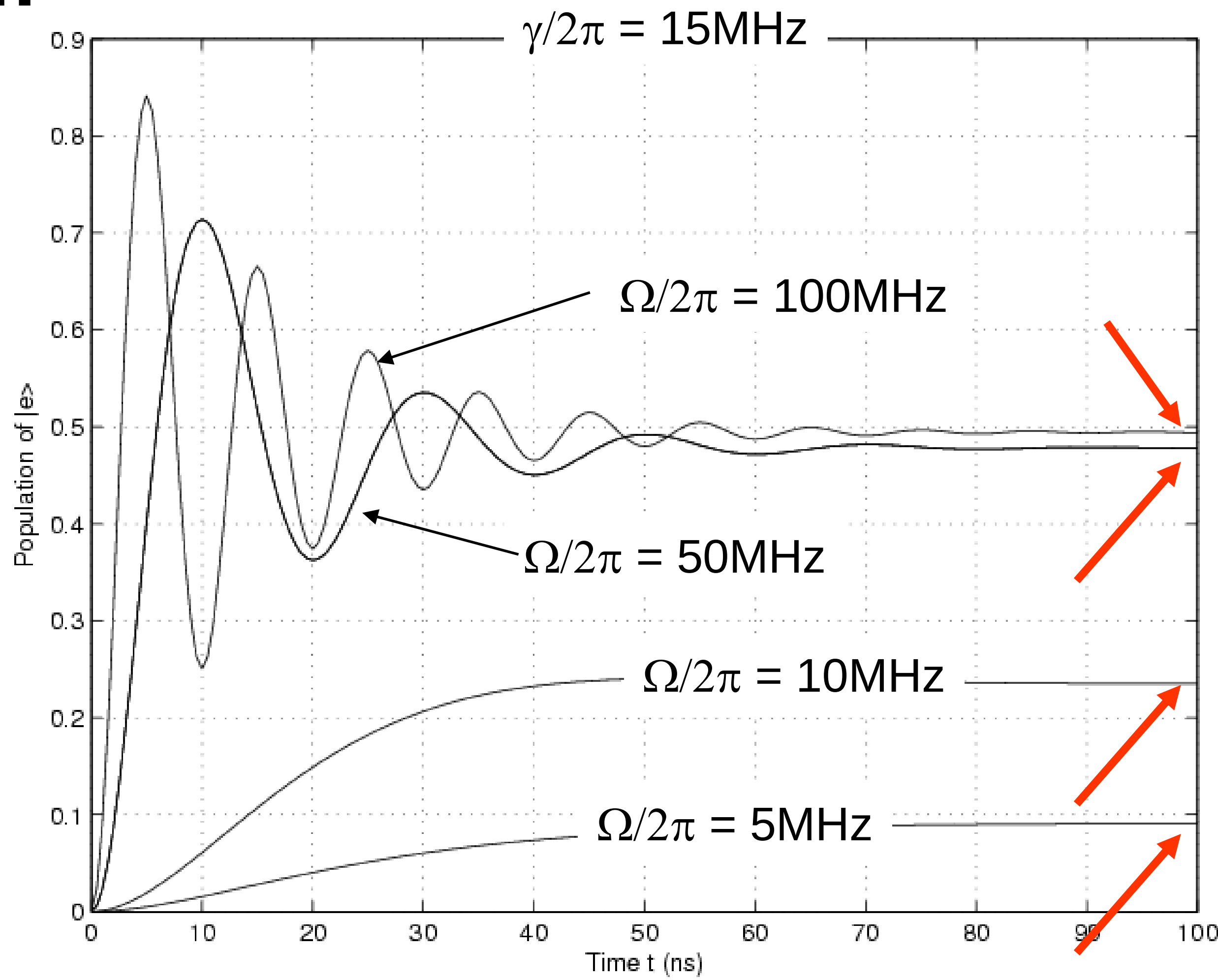

Steady state population of |e>:

$$\rho_{ee}(t \to \infty) = \frac{(\Omega/2)^2}{\Delta^2 + (\gamma/2)^2 + 2(\Omega/2)^2} \simeq \left(\frac{\Omega}{\gamma}\right)^2 \frac{1}{1 + (2\Delta/\gamma)^2} = \left(\frac{\Omega}{\gamma}\right)^2 W(\Delta)$$

Rate equations of absorption

excitation probabilities in pertubative regime:

incoherent excitation if $\Omega_{Rabi} << \gamma$

$$\rho_{ee}(t \to \infty) = \frac{(\Omega/2)^2}{\Delta^2 + (\gamma/2)^2 + 2(\Omega/2)^2}$$

$$\simeq (\frac{\Omega}{\gamma})^2 \frac{1}{1+(2\Delta/\gamma)^2} = (\frac{\Omega}{\gamma})^2 \; W(\Delta)$$

photon scatter rate: $S = \gamma \rho_{ee}$

spont. decay rate: γ

absorption

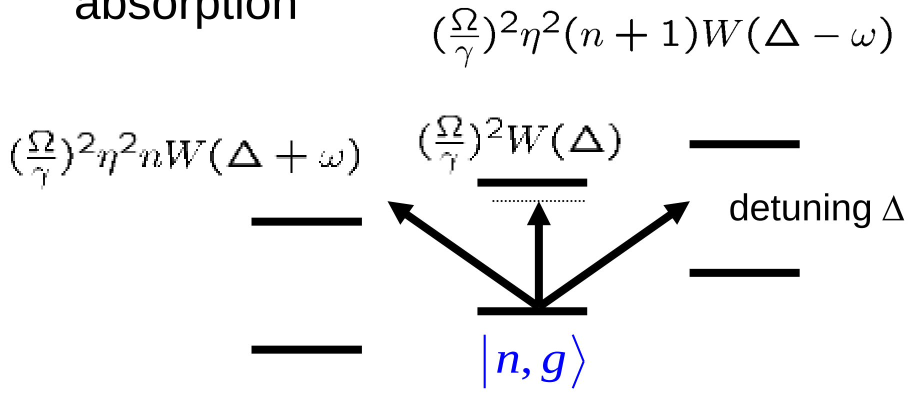

Rate equations of absorption and emission

excitation probabilities in pertubative regime:

incoherent excitation if $\Omega_{Rabi} << \gamma$

$$\rho_{ee}(t \to \infty) = \frac{(\Omega/2)^2}{\Delta^2+(\gamma/2)^2+2(\Omega/2)^2}$$

$$\simeq (\frac{\Omega}{\gamma})^2 \frac{1}{1+(2\Delta/\gamma)^2} = (\frac{\Omega}{\gamma})^2 \; W(\Delta)$$

photon scatter rate: $S = \gamma \rho_{ee}$

spont. decay rate: γ

emission

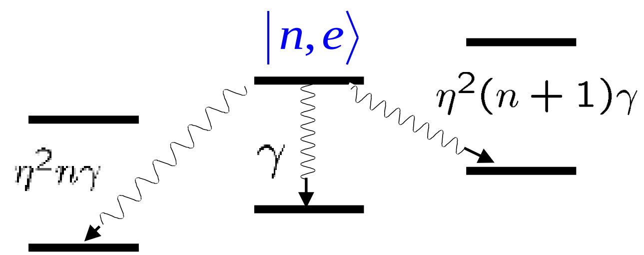

take all physical processes that change *n*, in lowest order of η

cooling:

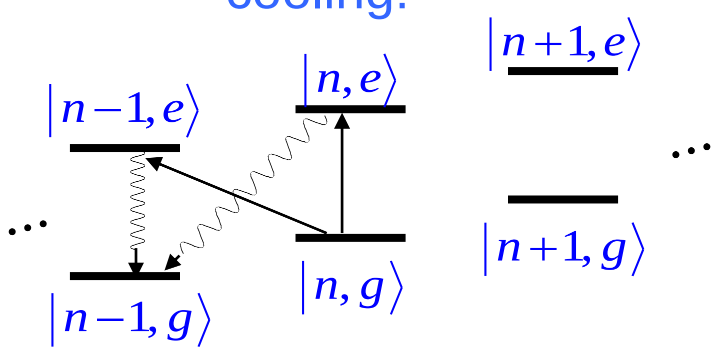

heating:

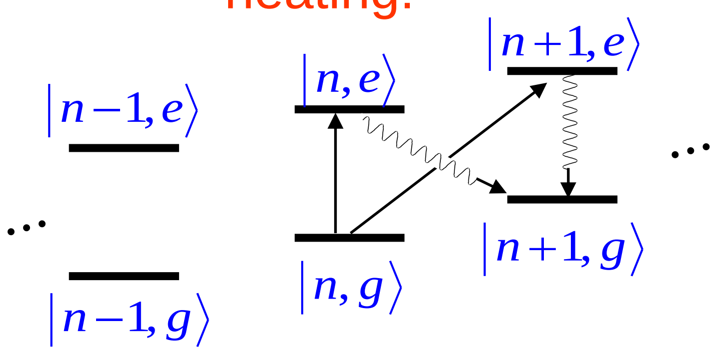

S. Stenholm, Rev. Mod. Phys. ***58****, 699 (1986)*

Rate equations for cooling and heating

cooling:

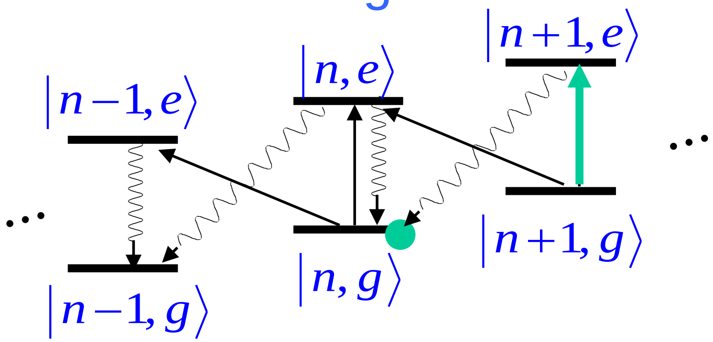

heating:

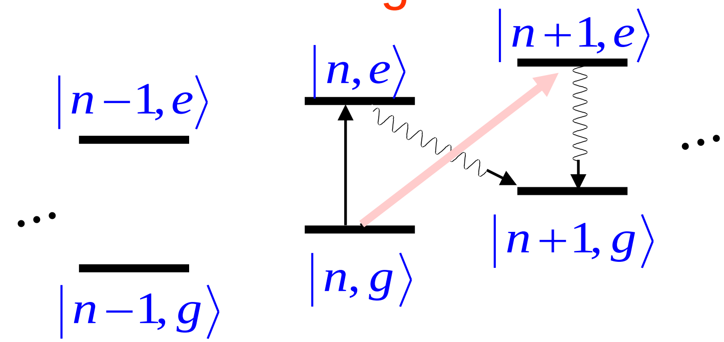

probability for population in |g,n>: loss and gain from states with |±n>

$$\dot{P}_{g,n} = \eta^2\gamma\left(\frac{\Omega}{\gamma}\right)^2 \cdot \left(\begin{array}{l|l} -nW(\Delta)P_n & -(n+1)W(\Delta)P_n \\ -nW(\Delta+\omega)P_n & \boxed{-(n+1)W(\Delta-\omega)P_n} \\ \hline \boxed{+(n+1)W(\Delta)P_{n+1}} & +nW(\Delta)P_{n-1} \\ +(n+1)W(\Delta+\omega)P_{n+1} & +nW(\Delta-\omega)P_{n-1} \end{array}\right) \begin{array}{l} \text{loss} \\ \\ \text{gain} \end{array}$$

cooling | heating

S. Stenholm, Rev. Mod. Phys. ***58****, 699 (1986)*

Rate equation

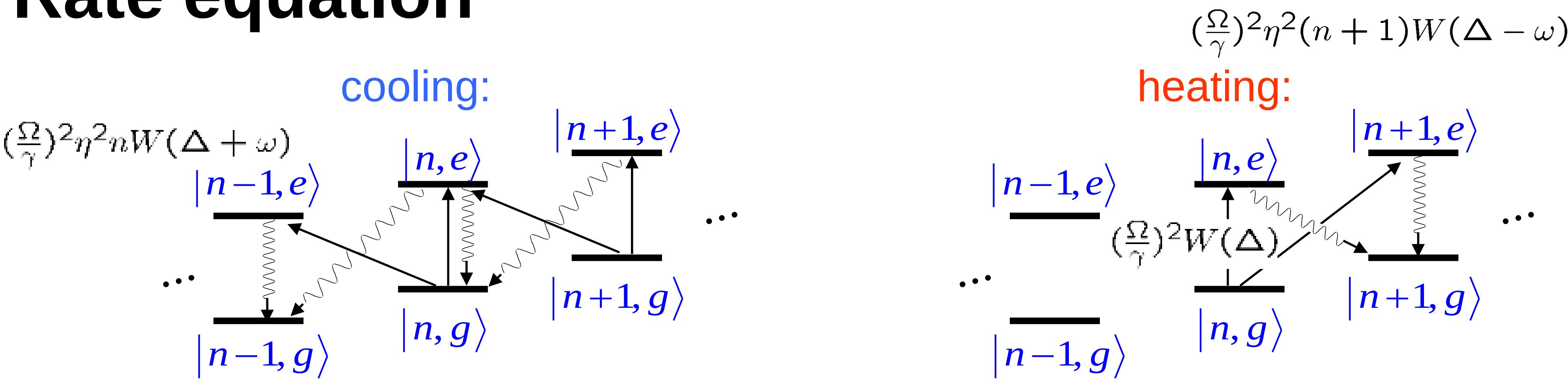

$$A_- = W(\Delta) + W(\Delta+\omega) \quad \text{cooling}$$
$$A_+ = W(\Delta) + W(\Delta-\omega) \quad \text{heating}$$
$$A_- - A_+ = W(\Delta+\omega) - W(\Delta-\omega)$$

different illustration:

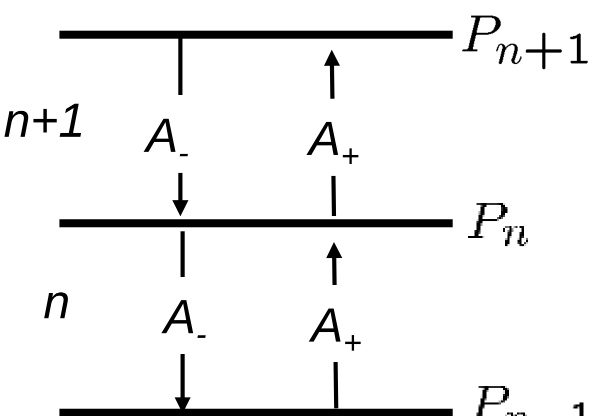

$$\langle \dot{n} \rangle = \frac{(\eta\Omega)^2}{\gamma} \sum n \frac{dP_n}{dt}$$
$$\Longrightarrow \quad \langle \dot{n} \rangle \sim -(A_- - A_+)\langle n \rangle + A_+$$
$$\langle n \rangle_{ss} = \frac{A_+}{A_- - A_+} \qquad 1/\tau_{cool} = \frac{(\eta\Omega)^2}{\gamma}(A_- - A_+)$$

steady state phonon number — cooling rate

How to reach $A_- > A_+ \Rightarrow W(\Delta+\omega) > W(\Delta-\omega) \Rightarrow$ red detuning $\Delta < 0$

***

$$\dot{m} = \langle \dot{n} \rangle = \sum n \ \frac{dP_n}{dt} =$$

$$\sum_{n=1} A_- P_{n+1}(n+1)(n) - A_- P_n(n)(n) + A_+ P_{n-1}(n)(n) \cdot A_+ P_n(n+1)(n)$$

$$= A_-(P_2 \cdot 2 \cdot 1 + P_3 \cdot 3 \cdot 2 + \ldots - P_1 \cdot 1 \cdot 1 - P_2 \cdot 2 \cdot 2 - \ldots)$$

$$+ A_+(P_0 \cdot 1 \cdot 1 + P_1 \cdot 2 \cdot 2 + \ldots - P_1 \cdot 2 \cdot 1 - P_2 \cdot 3 \cdot 2 - \ldots)$$

$$= A_-(P_1 - P_2 \cdot 2 - P_3 \cdot 3 \ldots)$$

$$+ A_+(P_0 + P_1 \cdot 2 - P_2 \cdot 3 - P_3 \cdot 4 \ldots)$$

$$= -A_- \sum n \cdot P_n \ + A_+ \sum (n+1) \cdot P_n$$

$$= -A_- \langle n \rangle + A_+ \langle n \rangle + A_+ \cdot \sum P_n$$

$$= -A_- \langle n \rangle + A_+ \langle n \rangle + A_+$$

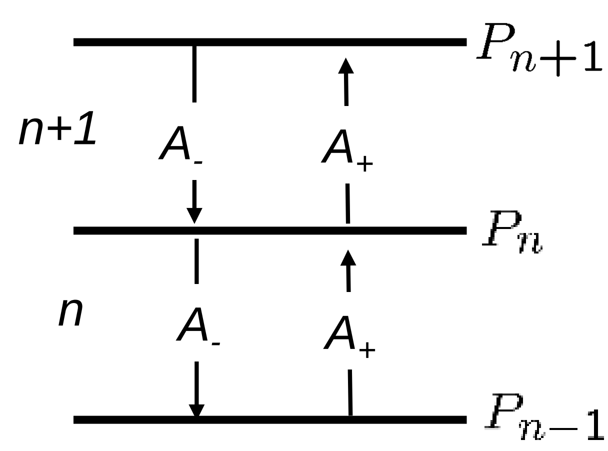

$$\langle \dot{n} \rangle = 0 \ \Longrightarrow \ \langle n \rangle = \frac{A_+}{A_- - A_+}$$

hurra !

„Weak confinement“

$$\boxed{\omega_{trap} << \gamma}$$

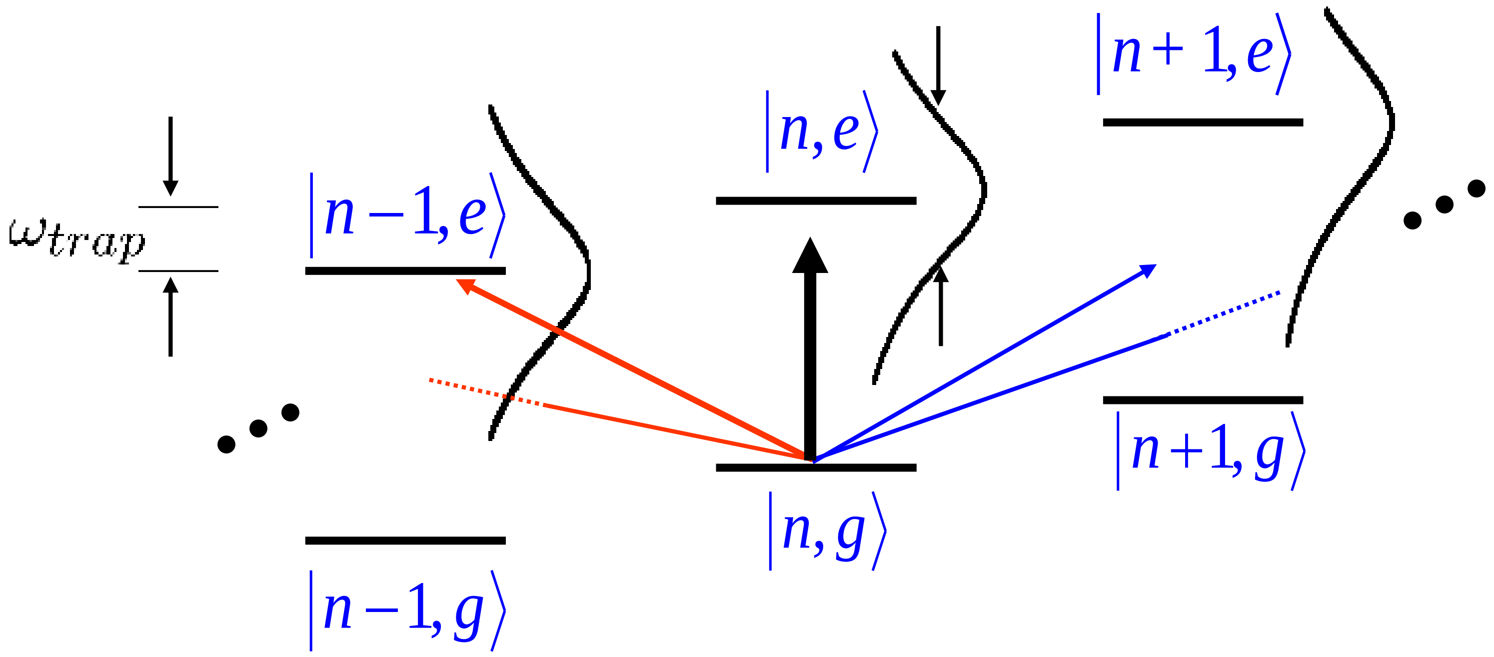

weak confinement:
Sidebands are not resolved on that transition.
Small differences in $W(\Delta \pm \omega), W(\Delta - \omega)$

detuning for optimum cooling $\Delta = -\gamma/2 \quad \Rightarrow \quad \langle n \rangle_{ss} = \frac{\gamma/2}{\omega_{trap}}$

„Weak confinement“

$$\boxed{\omega_{trap} << \gamma}$$

Lorentzian has the
steepest slope at $-\gamma/2$

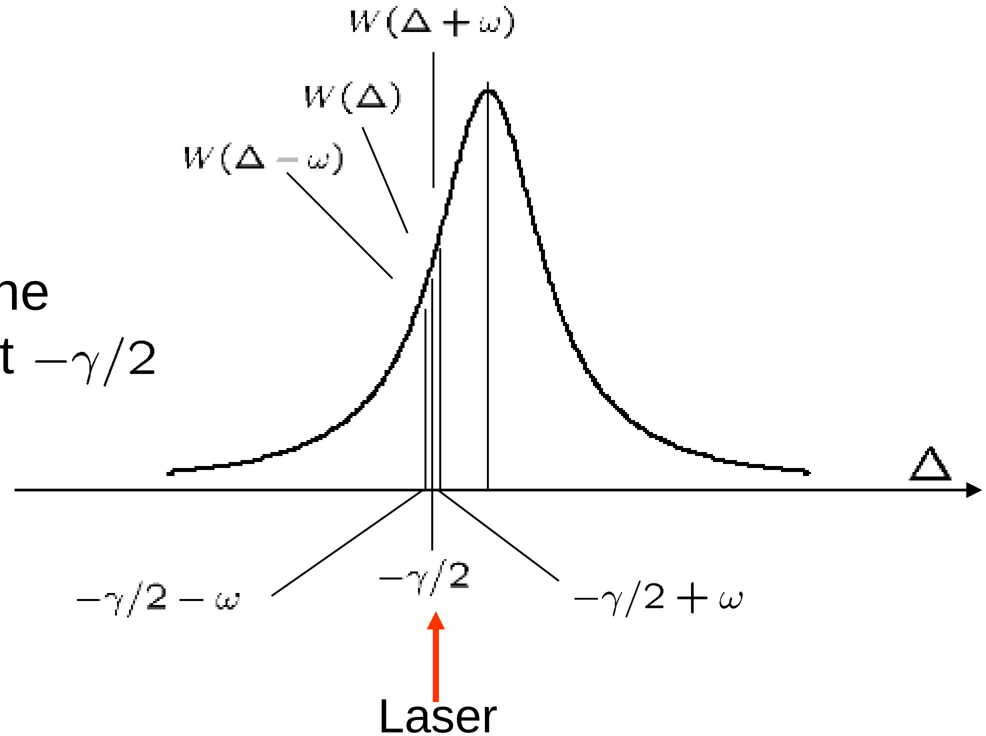

Doppler cooling

complications:

- $\eta_{laser} < \eta_{spontaneous}$
- saturation effects
- optical pumping

weak confinement:
Sidebands are not resolved on that transition.
Small differences in $W(\Delta \pm \omega), W(\Delta - \omega)$

$$\boxed{\text{detuning for optimum cooling } \Delta = -\gamma/2 \quad \Rightarrow \quad \langle n \rangle_{ss} = \frac{\gamma/2}{\omega_{trap}}}$$

„Strong confinement“

$$\boxed{\omega_{trap} >> \gamma}$$

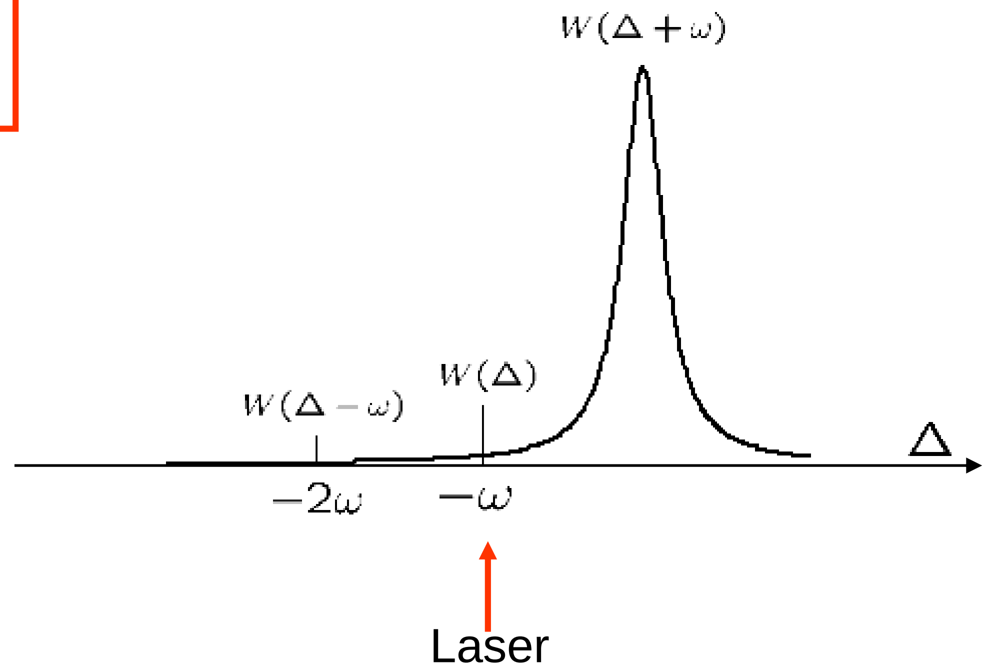

ground state cooling

strong confinement – well resolved sidebands:
detuning for optimum cooling

$$\boxed{\Delta = -\omega_{trap} \quad \Rightarrow \quad \langle n \rangle_{ss} \approx \left(\frac{\gamma/2}{\omega_{trap}}\right)^2 << 1}$$

„Strong confinement“

$$\boxed{\omega_{trap} >> \gamma}$$

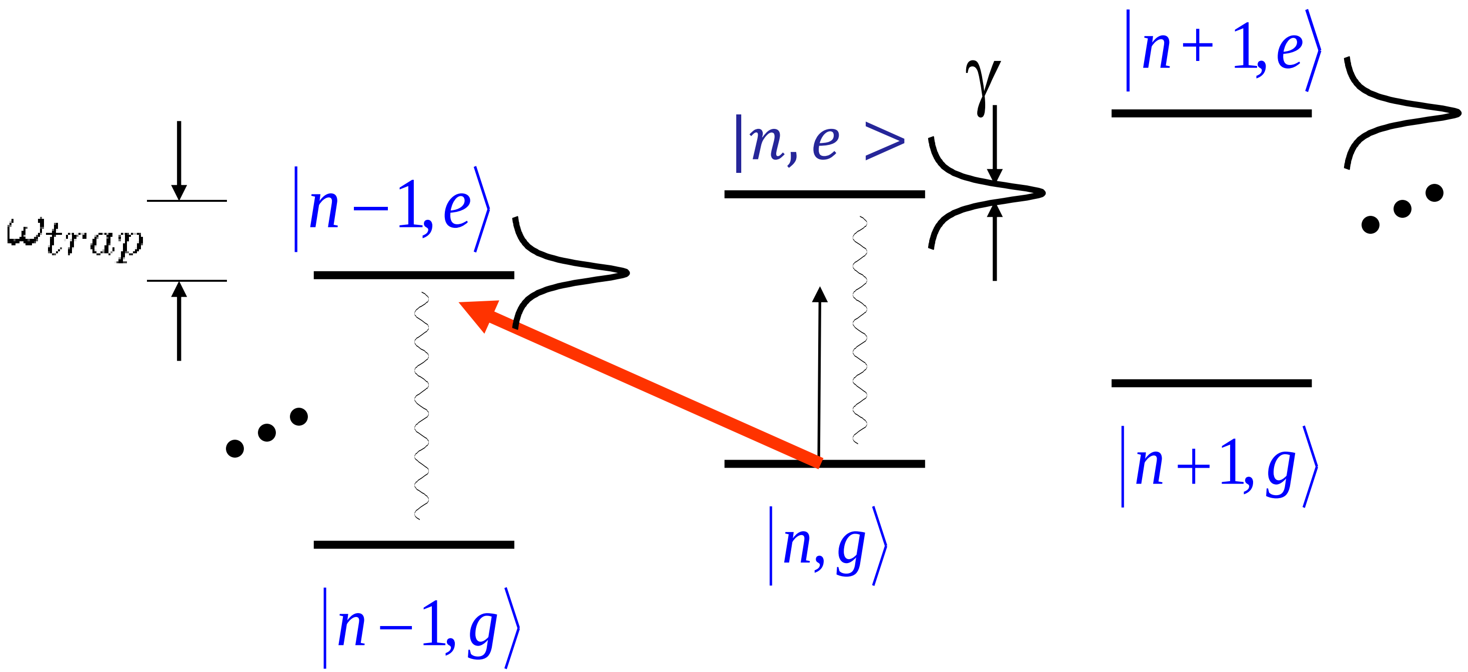

strong confinement – well resolved sidebands:
detuning for optimum cooling

$$\boxed{\Delta = -\omega_{trap} \;\Rightarrow\; \langle n \rangle_{ss} \approx (\frac{\gamma/2}{\omega_{trap}})^2 << 1}$$

Cooling limit

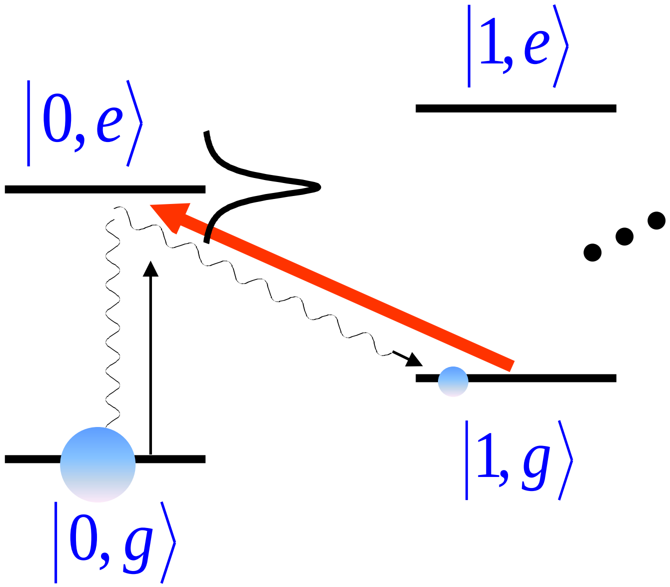

$$\Delta = -\omega_{trap}$$

Limit of SB cooling

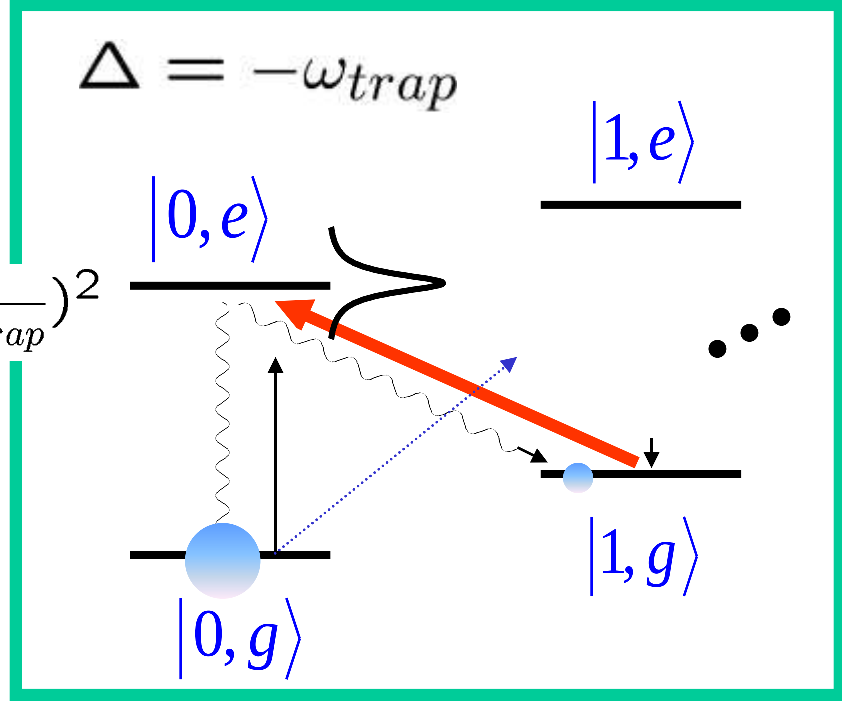

off resonant carrier excitation: $(\frac{\Omega}{\gamma_{eff}})^2 \frac{1}{1+(2\Delta/\gamma_{eff})^2} \overset{\Delta=-\omega_{trap}}{=} (\frac{\Omega}{2\omega_{trap}})^2$

subsequent blue SB decay: $\eta^2_{spont}\gamma_{eff}$
with an „effective" γ
and the η of spont. emission

leads to heating: $\eta^2_{spont}\gamma_{eff}\Omega^2/(2\omega_{trap})^2$

off resonant blue SB excitation $\Delta = -2\omega_{trap}$
leads to heating: $\gamma_{eff}\ (\eta_{laser}\Omega)^2/(4\omega_{trap})^2$

$$\boxed{\dot{p_0} = p_1\frac{(\eta_{laser}\Omega)^2}{\gamma_{eff}} - p_0\ (\frac{\Omega}{2\omega_{trap}})^2\eta^2_{spont}\gamma_{eff} - p_0\ (\frac{\eta_{laser}\Omega}{4\omega_{trap}})^2\gamma_{eff}, \quad \dot{p_0} = -\dot{p_1}}$$

with: $\dot{p_0} = 0, p_1 = 1 - p_0$

$$\boxed{n \approx p_1 \approx (\frac{\gamma_{eff}}{2\omega_{trap}})^2((\frac{\eta_{spont}}{\eta_{laser}})^2 + \frac{1}{4})}$$

typical experimental parameters: $n \approx (\frac{5kHz}{5MHz})^2((\frac{0.05}{0.02})^2 + \frac{1}{4}) \approx 5{\times}10^{-6}$

Resolved sideband spectroscopy

Select narrow optical transition with: $0.2..20 MHz \sim \omega_{trap} >> \gamma$

a) Quadrupole transition
b) Raman transition between Hyperfine ground states
c) Raman transition between Zeeman ground states
d) Octopole transition
e) Intercombination line
f) RF transition

Species and Isotopes:

for (a)	^{40}Ca, ^{43}Ca, ^{138}Ba, ^{199}Hg, ^{88}Sr, ...
for (b)	^{9}Be, ^{43}Ca, ^{111}Cd, ^{25}Mg....
for (c)	^{40}Ca, ^{24}Mg, ...
for (d)	$^{172/172}$Yb, ...
for (e)	^{115}In, ^{27}Al, ...
for (f)	^{171}Yb, ...

Level scheme of $^{40}Ca^+$

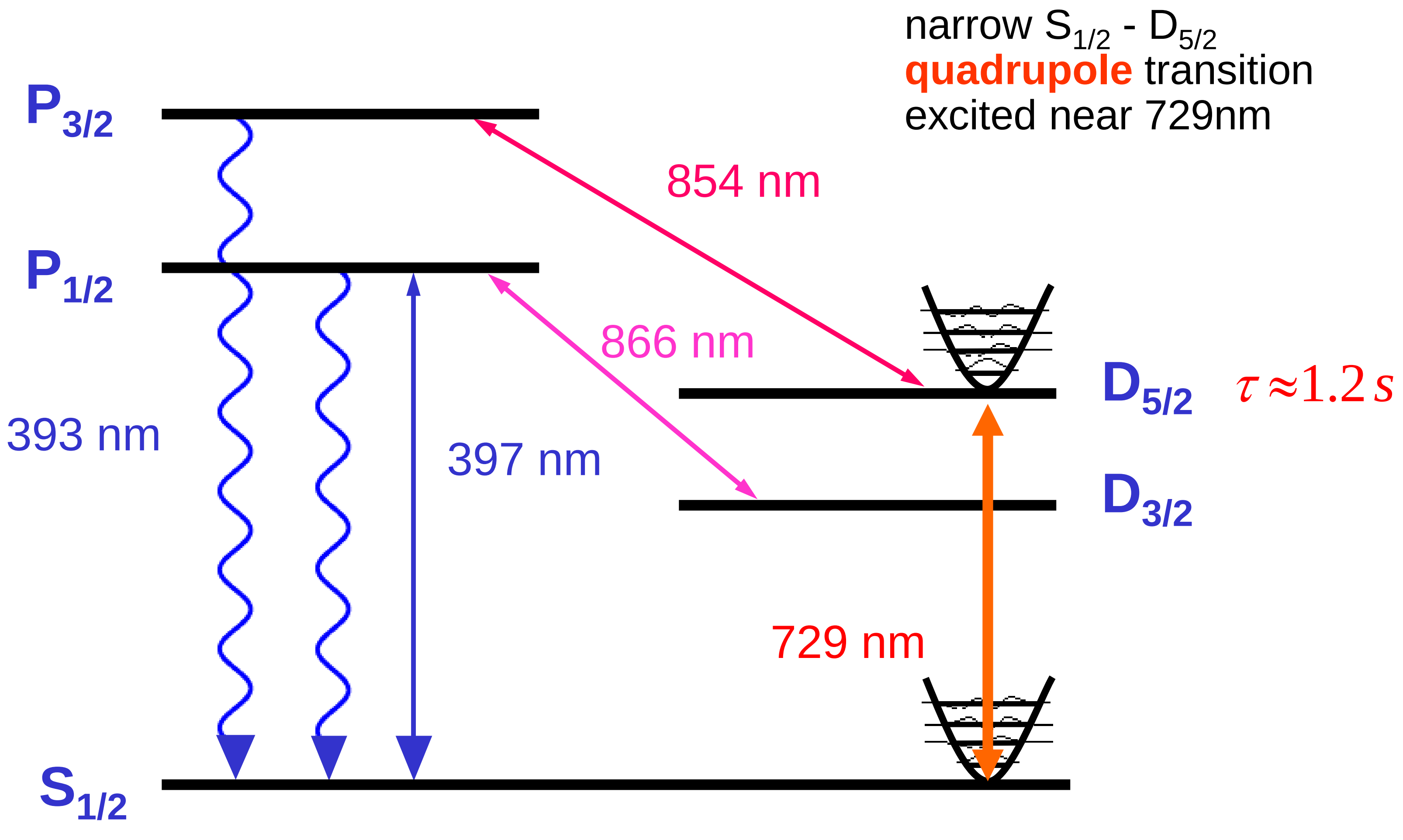

Ion energy levels

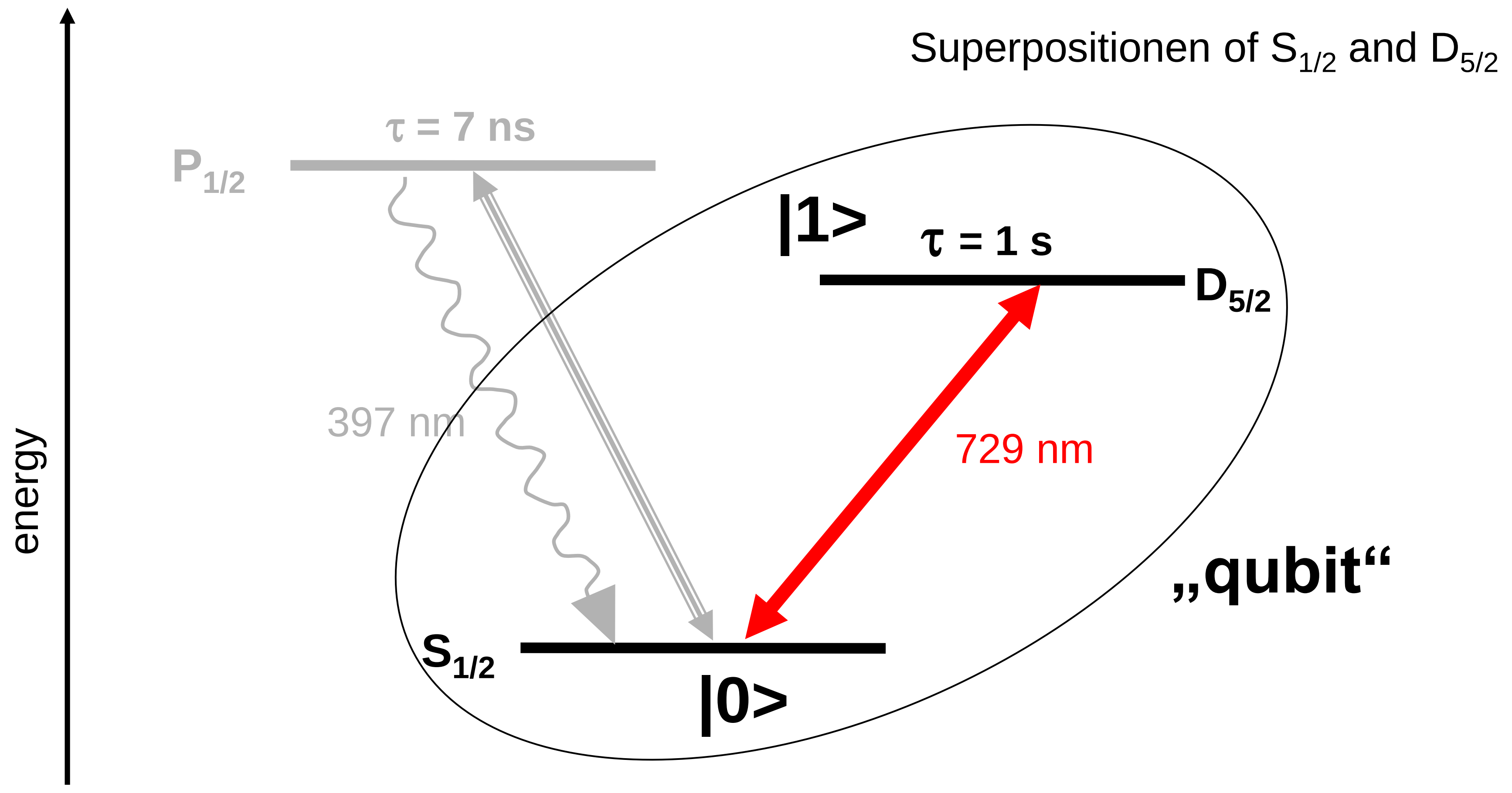

Ion energy levels

Specroscopy pulse followed by detection of qubits:

Scatter light near 397nm:
$S_{1/2}$ emits fluorescence
$D_{5/2}$ remains dark